Journal of
Composites Science

MDPI

Article

Adsorption in an Aqueous Multimetal System Using a Mineral–Biological Composite: A Kinetic and Isotherm Study

David Choque-Quispe [1,*], Jorge W. Elias-Silupu [2], Ybar G. Palomino-Malpartida [3], Wildor Merardo Díaz Bazán [4], Yakov Felipe Carhuarupay-Molleda [4], Bryan Jefferson Abollaneda Altamirano [5], Arturo Rojas Benites [4], Carlos Eduardo Dueñas Valcarcel [6], Carmen Rosa Cárdenas Rosales [7] and Edward Arostegui León [5]

1 Agroindustrial Engineering Department, José María Arguedas National University, Andahuaylas 03701, Peru
2 Science and Engineering Department, Ciro Alegria National University, Huamachuco 13301, Peru; jelias@unca.edu.pe
3 Chemical Engineering Department, San Cristobal de Huamanga National University, Ayacucho 05000, Peru; ybar.palomino@unsch.edu.pe
4 Basic Sciences Department, José María Arguedas National University, Andahuaylas 03701, Peru; wmdiaz@unajma.edu.pe (W.M.D.B.); ycarhuarupay@unajma.edu.pe (Y.F.C.-M.); arojas@unajma.edu.pe (A.R.B.)
5 Environmental Engineering Department, José María Arguedas National University, Andahuaylas 03701, Peru; bjabollaneda@unajma.edu.pe (B.J.A.A.); earostegui@unajma.edu.pe (E.A.L.)
6 Environmental Assessment and Enforcement Agency—OEFA, Lima 15027, Peru; cduenas.ing.amb@gmail.com
7 Civil Engineering Department, Universidad Nacional Autónoma de Chota, Cajamarca 06120, Peru; crcardenasr@unach.edu.pe
* Correspondence: dchoque@unajma.edu.pe

Abstract

Anthropogenic activities generate waste that negatively impacts the environment, especially water resources, due to the accumulation of heavy metal ions. Several adsorption methods have been developed, including the use of natural materials such as algae and activated clay. This study aimed to evaluate the effect of pH on batch adsorption of heavy metal ions using *Nostoc sphaericum* hydrocolloid (HA)/activated nanoclay (NR) composites. The NR/HMB-HA and NR/HUT-HA composites were prepared with a 2:8 mass ratio of HA and NR, using types of clay with code HMB and HUT, previously activated with 1 M NaCl and acid treatment. The adsorption capacity was evaluated using batch tests at pH 4.5 and 5.5, analyzing the removal percentage, adsorption kinetics, adsorption isotherms, and regeneration cycles for unimetal and multimetal systems. The composites present a load point close to 5.1. The FTIR analysis showed changes in the intensity of functional groups following adsorption, confirming the interaction with metallic ions. Both composites showed high affinity in multimetallic systems, especially at pH 5.5, with high selectivity for Pb^{2+} (≈99% removal), followed by As, Cd, and Zn, from an initial concentration of 10 ppm for each metal ion. Equilibrium is reached in approximately 90 min, allowing adsorption of up to 69.9% after five regeneration cycles in a multimetal system. The kinetic study showed that multimetal absorption at equilibrium is governed by chemisorption processes in the order Pb > As > Zn > Cd, with q_e values between 0.392 and 0.058 mmol/g and diffusivity from 15.506×10^{11} to 1.692×10^{11} m^2/s. Likewise, the isotherms study indicated a favorable process with maximum adsorption (q_{max}) between 16.696 and 5.223 mmol/g at pH 5.5. Altogether, the developed composites show high potential for the removal of heavy metals in contaminated waters, in addition to their high reuse capacity.

Check for updates

Academic Editors: Carlos Rafael Silva De Oliveira, Jéssica Mulinari and Afonso Henrique da Silva Júnior

Received: 10 February 2026
Revised: 19 February 2026
Accepted: 23 February 2026
Published: 26 February 2026

Copyright: © 2026 by the authors. Licensee MDPI, Basel, Switzerland. This article is an open access article distributed under the terms and conditions of the Creative Commons Attribution (CC BY) license.

Keywords: composite activated clay/hydrocolloid; chemisorption; unimetal and multimetal systems; *Nostoc sphaericum*

1. Introduction

Wastewater from mining, industrial activities, or even domestic sewage can reach rivers, lagoons, and other bodies of water. It is known that these effluents contain various organic and inorganic compounds. Among all the compounds present in the effluents, metals present a significant challenge in removal using conventional treatments.

Pollution by metallic ions is identified as one of the most relevant environmental problems due to its harmful effects on the environment and human health when it exceeds the levels established by current regulations. Due to its mobility in aquatic systems, its toxicity, and its bioaccumulative capacity, it can reach very high concentrations and cause toxic effects on aquatic life [1], which are difficult to remove through conventional treatment.

Conventional technologies for removing heavy metals from water, including physical and chemical processes, include precipitation, coagulation–flocculation, oxidation–reduction processes, ion exchange, and subsequent filtration. However, alternative separation methods such as adsorption, electrochemical treatments, reverse osmosis, and evaporation have been developed. Nevertheless, they can be expensive and relatively ineffective when it comes to removing or eliminating metals in low concentrations [2]. Furthermore, they generate residual sludge, the treatment and disposal of which constitute an additional expense to the purification process [3]. However, the proposal for materials that do not involve aggressive chemical and physical processes for their activation or use, and even more so if they are of biological or mineral origin with little use or high abundance, contributing to the circular economy, sustainability, and green chemistry, could minimize the cost of the technology.

Currently, new environmentally friendly technologies are being developed through the use of biopolymers from biomass waste and inorganic materials at the nanoparticulate level, activated by physical and chemical means. These technologies can reduce transition metal ion concentrations to parts per billion [4,5] because they present functional groups such as hydroxyl, carbonyl, carboxyl, and amine, or inserted cations, with a larger surface area and high porosity, which increase the efficiency of metal ion adsorption.

The absorption of metal ions using individual or synergistic compounds of biological and/or inorganic origin is an efficient alternative for wastewater treatment, especially when diluted. This is due to the low implementation costs and the possibility of recovering heavy metals from aqueous effluents, as well as ease of handling, environmental friendliness, low waste generation, and limited use of chemical-derived materials [4,5]. Bioadsorbents can be materials from microbial flora, algae, plants, biomass residues, and agro-industrial products [3,6]. Biopolymers, as an alternative for metal removal, are advantageous due to their low cost and ease of handling.

Biopolymers are promising for metal removal [7–9], as they contain high levels of starch and proteins, which have chelating capacity, and can remove heavy metals from contaminated water, in addition to being obtained from renewable sources [7–10].

Numerous studies have been conducted on the use of natural and residual biomass due to its economic advantages. These biomasses are enhanced through physical and/or chemical activation, reporting adsorption rates exceeding 80% in multimetal systems. Similarly, the use of activated clays offers advantages in metal ion removal due to their high surface area and cation exchange capacity, which have been the subject of numerous studies. Algae have become a promising research material due to their wide availability

and the presence of functional groups with high affinity and adsorption capacity, such as *Ulva flexuosa*, *Argassum wightii*, *Sargassum*, *Chlorella vulgaris*, *Nostoc muscorum*, and *Nostoc commune* [11–13]. The biopolymer *Nostoc sphaericum*, popularly known in Peru as Murmunta, Nostoc, Llullucha, Chusuro, and Crespito, has qualities that make it promising in the removal of metals [14].

The formulation of nanocomposites allows for the optimization of material use, as well as increased effectiveness in their application, especially in the removal of metals from wastewater. For example, clays have been used in water treatment for the removal of heavy metals [5]. Materials with a more ecological appeal allow for the sustainable development of communities, particularly in areas where environmental impact is evident, even more so in more sensitive areas such as the Andean highlands.

On the other hand, it is essential to know and understand the adsorption processes. This is possible through the study of isotherms and adsorption kinetics. These studies provide information on the efficiency and mechanisms of adsorbents, and from them, effective water treatment technologies can be developed [15,16]. This is subject to system parameters; thus, pH determines metal speciation and protonation of the adsorbent's functional groups. Salinity controls ionic strength and competition of dissolved cations for active sites. The zero charge point (pH_{ZCP}) defines the net surface charge and therefore electrostatic attraction or repulsion. The zeta potential (ζ) evaluates colloidal stability and the tendency to aggregate. Particle size conditions the available specific area and intraparticular diffusion. Cation exchange capacity (CEC) reflects the availability of active sites, while crystallinity, determined by XRD, indicates the structural order and accessibility of the pores [17,18]. The study of these parameters provides important information about adsorption mechanisms, the time required to reach equilibrium, the factors that influence efficiency (temperature, pH, and concentration), and the characteristics of the adsorbent surface.

One of the critical parameters during the metal ion adsorption process is pH. pH is responsible for the surface and internal chemistry of adsorbents, allowing the protonation and deprotonation of their functional groups. This directly influences the modification of the zeta potential (ζ), ZCP, colloidal stability, aggregation, and hydrodynamic particle size (adsorbent), as well as intraparticle diffusion. Simultaneously, in the adsorbent–adsorbate–aqueous medium system, pH allows for the specification of metal ions, whose adsorption is conditional upon reaching the ZCP, thus determining complexation, hydrolysis, and ion exchange [19–22].

In this context, we propose the use of an alternative, natural, and renewable adsorbent, such as the composite formed by the hydrocolloid Nostoc (*Nostoc sphaericum*) and activated nano-clay, for the purpose of removing heavy metals in batches at pH levels below and above the ZCP of the composites, which will enable the development of a new material for wastewater treatment.

2. Materials and Methods

2.1. Nostoc sphaericum Hydrocolloid Extraction (HA)

Samples of Nostoc were collected from the Puccacocha lagoon located at an altitude of 4251 m with coordinates 13°47′52″ S and 73°17′5″ W, in the province of Andahuaylas, Apurímac, Peru.

The methodology proposed by Choque et al. [23] was followed. Samples of fresh Nostoc (1.0 kg) were ground in a blender, then sieved through a 45-micron sieve. The resulting broth was then subjected to a spray dryer (model B-290, Büchi Labortechnik AG, Flawil, Switzerland) with an inlet temperature of 100 °C, an air flow rate of 600 L/h, and a suction speed of 38 m^3/h, obtaining the powdered hydrocolloid (HA).

For the analysis of the characteristics of HA, 50 g were placed in a tray dryer at 60 °C for 24 h, then placed in a desiccator for 24 h. The samples were then collected in HDPE bags and stored under ambient conditions in the dark. The dried samples were characterized by FTIR, total organic carbon (TOC), zeta potential (ζ), zero charge point (pH_{ZPC}), particle size, and XRD analysis.

2.2. Treatment and Activation of Nanoclay (NR)

Natural clays were collected in the districts of Huancabamba (HMB) (with coordinates 13°43′58.90″ S, 73°20′38.17″ W and an altitude of 3682 m) and Huanta (HUT) (with coordinates 12°53′37.09″ S, 74°15′57.65″ W and an altitude of 2720 m) in the provinces of Andahuaylas and Ayacucho, respectively, Peru.

The HUT and HMB natural clays were ground in a Retsch brand (Haan, Germany) PM100 planetary mill at 250 rpm for 10 min and then sieved to 125 microns. The sieved material was treated with 10% phosphoric acid to remove organic matter at a ratio of 1.0 g clay/4.0 mL acid and stirred at 300 rpm at 60 °C for 6 h; then it was rinsed with ultrapure water to pH 7, and dried at 60 °C. The clay was then activated with a 1.0 M NaCl solution at a ratio of 1.0 g of clay/5.0 mL and stirred at 200 rpm for 24 h. It was then rinsed with ultrapure water until a conductivity of less than 10 µS/cm of the residual water was achieved, and dried at 60 °C, obtaining the activated clay. The natural and activated clays were characterized by FTIR spectroscopy, SEM surface characterization, cation exchange capacity (CEC), total organic carbon, zeta potential (ζ), zero charge point (pH_{ZPC}), particle size, and XRD analysis.

2.3. Composite Preparation

HA was mixed with clay and nanoclay in the proportions shown in Table 1. The mixtures were pressed to obtain tablets for easy handling and weighing.

Table 1. Experimental design matrix.

Treatment	Composite	
	HA	**NR**
HMB-HA	20%	80%
NR/HMB-HA	20%	80%
HUT-HA	20%	80%
NR/HUT-HA	20%	80%

Where HA is atomized *Nostoc sphaericum*, NR/HMB is activated HMB clay, NR/HUT is activated HUT clay, HUT and HMB are types of clay.

The prepared composites were characterized by zero charge point (pH_{ZPC}), SEM, and FTIR analysis.

2.4. Physical and Chemical Properties of Materials for the Production of Composites

2.4.1. Determination of Total Organic Carbon (TOC)

The TOC and inorganic carbon (IC) in natural clay, NR, and HA were determined by high-temperature combustion, and the CO_2 produced was determined by non-dispersive infrared spectroscopy, using a Shimadzu SSM-5000A model (Tokyo, Japan).

2.4.2. Determination of Cation Exchange Capacity (CEC)

The CEC of natural clay and NR was determined by summing the compulsory exchanges of Al, Ca, Mg, K, and Na for Ba. In this method, exchangeable cations are removed with a 0.1 mol/L $BaCl_2$ solution by centrifugation for 2 h, and the ion concentration is

determined by ICP-OES (model 9820, Shimadzu, Tokyo, Japan). The CEC value (cmol/kg) is equal to the sum of the cations [24,25].

2.4.3. Particle Size and Zeta Potential (ζ) Determination

Four mg of the dry sample (natural clay, NR, and HA) was weighed and dispersed in 5 mL of ultrapure water, stirred at 1000 rpm for 5 min, then ultrasonicated for 10 min at room temperature. An aliquot was taken in a capillary, and the hydrodynamic diameter and size distribution were determined by dynamic light scattering (DLS) using the Zetasizer ZSU3100 instrument (Malvern Instruments, Worcestershire, UK) with a bandwidth of 33 µsec and a scattering angle of 90°.

Similarly, 2 mL was loaded into a polystyrene cell and read on the same instrument, with a laser wavelength of 632.8 nm, a scattering angle of −14.14°, and an electric field intensity of 5 V/cm.

2.4.4. Zero Charge Point Determination (ZCP)

Solutions with pH 2 to 12 were prepared using 1 M NaOH and 1 M HCl for the tests and ZCP determination. Then, 0.05 g of the samples (natural clay, NR, HA, and composite) was added to 50 mL of each solution and subjected to continuous stirring at 150 rpm for 24 h at environment. At the end, the pH of the resulting solution was measured [26]. To find the PZC, the initial pH values were plotted against the final pH of the solution; the intersection between the curves indicates the PZC value.

2.5. Structural Properties of Materials

2.5.1. Crystalline Properties

X-ray diffraction analysis of the materials was performed using a Bruker D8-Focus diffractometer (Cu Kα1 = 1.5406 Å) at 40 kV and 40 mA (Bruker, Karlsruhe, Germany), with a LynxEye PSD detector. Scattered radiation was detected in the angular range of 4–70° (2θ) and a step of 0.04°.

The degree of crystallinity (*DC*) was determined by the ratio between the area corresponding to the crystalline phase and the total area under the XRD curve (Equation (1)) [27].

$$DC\ (\%) = \frac{S_{cr.p}}{S_t} \times 100, \quad (1)$$

where $S_{cr.p}$ is the area corresponding to the crystalline phase, and S_t is the total area of the diffractogram.

The size of the crystals (*D*) was determined from the diffractogram using the Scherrer equation [28].

$$D = \frac{k_{DRX} \cdot \lambda}{\beta \cdot cos\theta}, \quad (2)$$

where k_{DRX} is the Scherrer constant (0.9); λ is the wavelength of the X-ray source (0.15406 nm); β is the peak angle of the diffraction peak profile at half the maximum height resulting from the small size of the crystals (in radians); θ is the peak position (in radians).

2.5.2. Functional Groups Determination

Tablets containing 0.1% of each material and composite in IR-grade KBr were prepared and placed in the transmission module of the Thermo Fisher Nicolet IS50 FTIR spectrometer (Waltham, MA, USA), in a range of 4000 to 400 cm^{-1} with a resolution of 4 cm^{-1}.

2.5.3. Surface Characterization

The material samples were prepared with 12.0 mm carbon adhesive disks with a 12.7 × 8.0 mm aluminum support. The analysis was performed under low vacuum at a pressure of 0.07 Torr. Micrographs were observed at 5000× magnification at a distance of 10 mm using a Thermo Fisher Prisma E scanning electron microscope (Brno, Czech Republic).

2.6. Evaluation of Metal Adsorption

Starting from a standard solution of 1000 ppm of Pb ($Pb(NO_3)_2$ in 2% HNO_3), As (As_2O_3 in 2% HNO_3), Cd ($Cd(NO_3)_2$ in 2% HNO_3) and Zn ($Zn(NO_3)_2$ in 2% HNO_3) from the Scharlau brand (Spain), a multimetal solution of 10 ppm of the metal ions (Pb^{2+}, As^{3+}, Cd^{2+} and Zn^{2+}) was prepared by dilution with deionized water, the pH was subsequently adjusted with 0.1 M NaOH.

Then, 5 mg of composite in its different formulations (Table 1) was immersed in 50 mL of solution under continuous stirring at 50 rpm for 24 h at environmental conditions. An aliquot filtered through a 0.45 µm hydrophobic filter was taken at the end of the time to be analyzed using an ICP-OES 9820 Shimadzu (Tokyo, Japan), previously calibrated with standards for each metal (STD calibration solution, SCP Science). Sample readings were performed in axial mode, in quadruplicate, with a 30 s rinse between samples at 60 rpm, a gas flow rate of 10 L/min, and a 30 s plasma exposure. The absorption capacity of the polymer was determined by the concentration difference in triplicate and expressed as a percentage of removal and adsorption capacity in equilibrium (q_e).

2.7. Adsorption Kinetics Evaluation

Briefly, 250 mL of multimetal solutions of Pb^{2+}, As^{3+}, Cd^{2+}, and Zn^{2+} were prepared and added to 25.0 mg of composite, stirring at 50 rpm at room temperature, for contact times of 0, 5, 10, 30, 60, 90, 120, and 150 min. For each time, an aliquot was filtered and subjected to ICP-OES. The experimental adsorption for single-metal and multimetal systems, over time ($q_{t,e}$), was determined using Equation (3) [29].

$$q_{t,e} = \frac{V(C_0 - C_t)}{m}, \tag{3}$$

where C_t (mmol/L) is the concentration of the metal at time t, C_0 (mmol/L) is the initial concentration of the metal at t = 0 min, V (L) is the volume of the solution, and m (mg) is the mass of the composite.

The kinetic behavior is evaluated using the following models:

2.7.1. Pseudo-First-Order Kinetic Model (PFO)

This was the first equation (Equations (4) and (5)) that allowed the description of the adsorption of a liquid system based on the capacity of a solid. It is based on the difference between the adsorption capacity at equilibrium and that obtained at a given time t. It is applicable during the first few minutes of the adsorption process [30,31].

$$\frac{dq_t}{dt} = k_1(q_e - q_t), \tag{4}$$

Integrating the equation, for time t = 0 to t = t, the metal concentration in the adsorbent is q = 0 to $q = q_t$, and has the form,

$$q_t = q_e\left(1 - e^{-k_1 t}\right), \tag{5}$$

2.7.2. Pseudo-Second-Order Kinetic Model (PSO)

This model primarily describes the chemical interaction between adsorbent and adsorbate (Equation (6)). It also considers that adsorption depends on the concentration of active sites [31–33].

$$\frac{dq_t}{dt} = k_2(q_e - q_t)^2, \tag{6}$$

Considering the boundary conditions of the pseudo-first-order equation, we obtain,

$$q_t = \frac{q_e^2 k_2 t}{1 + q_e k_2 t}, \tag{7}$$

2.7.3. Elovich Kinetic Model

This model applies to chemisorption processes (Equation (8)) and defines that the active sites of the adsorbent are heterogeneous, which generates different activation energies, based on a heterogeneous reaction mechanism [31,34].

$$q_t = \frac{1}{\beta}\ln(\alpha \cdot \beta) + \frac{1}{\beta}\ln(t), \tag{8}$$

2.7.4. Intraparticle Diffusion Kinetic Model (ID)

The model is based on Fick's laws of diffusion. In the model (Equation (9)), the probability of the adsorbate being transported from a concentrated zone to the adsorbent by diffusion is considered, generally for batch agitation processes, where adsorption varies almost proportionally to t1/2 instead of the contact time t [35–37].

$$q_t = k_i t^{1/2} + C, \tag{9}$$

If $C = 0$, the only control step is intraparticle diffusion; if $C \neq 0$, the adsorption process is complex and involves more than one diffusive resistance in the adsorbent.

2.7.5. Crank Diffusion Model

Adsorption in porous materials is characterized by slow mass transfer within the pore spaces, which is characterized by an intraparticle diffusion coefficient De. Thus, for long adsorption times, the model is represented by Equation (10) [38,39].

$$q_t = q_e\left(1 - \left(\frac{6}{\pi^2}\right)\exp\left(\frac{-D_e\pi^2 t}{r^2}\right)\right), \tag{10}$$

where q_e (mmol/g) is the adsorption capacity at equilibrium.; q_t (mmol/g) is the adsorption capacity at time t; k_1 $\left(\text{min}^{-1}\right)$ is the kinetic constant of the PFO model; t (min) is the contact time; k_2(g/mmol.min) is the kinetic constant of the PSO model; α (mmol/g.min) is the initial adsorption rate; β (mmol/g.min) is the parameter that can take a value between 0 and 1, which is related to the surface area covered and the activation energy by chemisorption; k_i (mmol/g.min$^{1/2}$) is the constant intraparticle diffusion rate; C (mmol/g) is a constant in the model; and D_e (m^2/s) is the intraparticle diffusion coefficient.

2.8. Adsorption Isotherms Evaluation

Briefly, 250 mL of the single-metal and multimetal solutions with concentrations of 10, 50, 100, 150, 200, and 250 ppm (adsorbate) were prepared, added to 25 mg of composite, and stirred at 50 rpm at 20 °C. A contact time of 90 min was considered to guarantee adsorption equilibrium; this was defined after preliminary kinetic tests, where it was

observed that equilibrium was reached around 60 min. Then, an aliquot was filtered (0.25 μm filter) and taken to ICP-OES.

The behavior of the isotherms was evaluated using the models below.

2.8.1. Langmuir Isotherm

The Langmuir isotherm model assumes that the surface of the adsorbent contains several active sites at the monolayer level, where the adsorbate adheres, and the adsorption energy is constant [40–42]. The model in its nonlinear form is:

$$q_e = \frac{q_m k_L C_e}{1 + k_L C_e}, \tag{11}$$

The affinity between adsorbate and adsorbent can be evaluated by the dimensionless separation factor R_L (Equation (12)). Thus, if $R_L > 1$, the relationship is unfavorable (little or no adsorbate adsorbed). $R_L = 1$ denotes a linear relationship; $0 < R_L < 1$ denotes a favorable relationship (good affinity between the adsorbate and the adsorbent, facilitating adsorption and retention of the adsorbate); and $R_L = 0$ denotes an irreversible relationship (the bonds between the adsorbent and the adsorbate are so strong that the adsorbate cannot be easily desorbed and remains permanently retained).

$$R_L = \frac{1}{(1 + k_L C_0)}, \tag{12}$$

To analyze the competitive effect of metal ions in the multimetal system, the affinity constant for active sites ($k_{L,i}$) was determined from the competitive Langmuir model.

$$q_e = \frac{q_{m,i} k_{L,i} C_{e,i}}{1 + \sum_{j=1}^{n} k_{L,j} C_{e,j}}, \tag{13}$$

2.8.2. Freundlich Isotherm

The Freundlich isotherm model describes heterogeneous reversible adsorption systems and is not limited to the formation of monolayers. The nonlinear form of this isotherm is given by [40,42,43],

$$q_e = k_f C_e^{1/n}, \tag{14}$$

2.8.3. Redlich–Peterson Isotherm

The Redlich–Peterson isotherm model explains the heterogeneity of adsorbents due to the energy distribution of their adsorbent sites. It is formulated by combining the Langmuir and Freundlich models and allows for the representation of equilibrium over a wide range of adsorbate concentrations. The model is represented in the form [44],

$$q_e = \frac{k_R C_e}{1 + a_R C_e^g}. \tag{15}$$

2.8.4. Temkin Isotherm

The Temkin isotherm model Assumes that the heat of adsorption of all molecules in the layers decreases linearly due to adsorbate–adsorbent interactions, and adsorption is characterized by the uniform distribution of binding energies up to a maximum energy. The non-linear form of this isotherm is given by [45–47],

$$q_e = \frac{RT}{b_t} \ln(A_t C_e), \tag{16}$$

where q_e (mmol/g) is the equilibrium adsorption capacity; k_L (L/mmol) is the Langmuir constant; C_e (mmol/L) is the concentration of adsorbate at equilibrium; q_m (mmol/g) is the adsorption capacity of the monolayer; C_o (mmol/L) is the initial concentration of the solution; K_f (mmol$^{1-1/n}$/L^n) and n are Freundlich constants, indicators of adsorption capacity and adsorption intensity, respectively; k_R (L/g) is the parameter that indicates the maximum adsorption capacity, a_R ((L/mmol)^g), and g is the constant parameter of the Redlich–Peterson model; R is the universal gas constant (8.314 J/mol.K); T (K) is the temperature; b_T (J/mol) is the variation in adsorption energy; A_T (L/mmol) is the equilibrium binding constant corresponding to maximum binding.

2.9. Adsorbent Regeneration Cycle

After the adsorption test, for a contact time of 90 min, the adsorbent was recovered by filtration through a 0.22 µm filter. The retentate was rinsed with copious amounts of distilled water and dried at 60 °C. The recovered adsorbent was desorbed in 0.1 M HCl and stirred continuously at 60 rpm for 60 min. It was then recovered by filtration, rinsed with deionized water, and dried. The adsorption process was then carried out following the steps detailed in Section 2.6. This operation was repeated five times [48,49].

2.10. Adjustment of Kinetic and Isothermal Models and Statistical Techniques

The parameters of the kinetic and isothermal models were determined using non-linear regression, and the least squares difference was fitted to the experimental data using the convergence criterion, evaluated by the Quasi-Newton method [50].

To numerically discriminate the models from the experimental data, the R^2 adjustment coefficient was calculated, which measures the variability of the dependent variable of the fitted model; the average relative error (*ARE*), which allows for minimizing the distribution of the fractional error; and the Chi-square test (X^2), which measures the difference in the squares of the experimental data with the data fitted by the model. The hybrid fractional error function (*HYBRID*) additionally includes a divisor as a term for the number of degrees of freedom of the system (the number of data minus the number of parameters within the model). The Marquardt percent standard deviation function (*MPSD*) is based on the geometric mean distribution of the error, which is modified to allow for the number of degrees of freedom of the system.

$$ARE = \frac{100}{N}\sum_{i=1}^{N}\left|\frac{q_{adj}-q_{exp}}{q_{exp}}\right|_i, \quad (17)$$

$$X^2 = \sum_{i=1}^{N}\left[\frac{\left(q_{exp}-q_{adj}\right)^2}{q_{adj}}\right]_i, \quad (18)$$

$$HYBRID = \frac{100}{N-n}\sum_{i=1}^{N}\left[\frac{\left(q_{adj}-q_{exp}\right)^2}{q_{exp}}\right]_i, \quad (19)$$

$$MPSD = 100\sqrt{\frac{1}{N-n}\sum_{i=1}^{N}\left[\frac{\left(q_{adj}-q_{exp}\right)^2}{q_{exp}}\right]_i}, \quad (20)$$

where q_{adj} is the adsorption capacity reported by the model, q_{exp} is the experimental adsorption capacity, N corresponds to the number of data points, and n is the number of model parameters.

R^2 values close to unity indicate a good model fit, while for *ARE*, X^2, *HYBRID*, and *MPSD*, they should be as low as possible [51–53].

The data was collected in triplicate, and the arithmetic mean ($\bar{x}$), standard deviation ($\pm$s), and coefficient of variability (CV) were determined. To evaluate the effects of input factors, ANOVA was applied, along with Tukey's multiple comparison test to identify significant differences at a 5% significance level. Data were analyzed using Excel calculation sheets and OriginPro 2025.

3. Results and Discussion

3.1. Composites Characterization

3.1.1. Individual Materials' Cationic Exchange Capacity

Cation exchange capacity (CEC) reflects the negative charges of clay and its ability to adsorb and exchange cations, constituting a predictive parameter for metal extractability [54,55]. Natural HUT clay exhibited a CEC of 10.47 $\pm$ 0.52 cmol/kg, higher than that of HMB (4.95 $\pm$ 0.17 cmol/kg) (Table 2). However, activation with NaCl significantly increased the CEC, an effect attributed to the exchange of Ca^{2+} for Na^{+}, which activates adsorption sites, improves thixotropic behavior, increases surface area, swelling, and metal adsorption capacity through physical, chemical, and ion exchange mechanisms [56–60].

Table 2. Characteristics of clays and HA.

Raw Materials and Composites	CEC (cmol/kg)				TOC (% *w*/*w*)				IC (% *w*/*w*)			ζ (mV)
	$\bar{x}$	±s	CV	*	$\bar{x}$	±s	CV	*	$\bar{x}$	±s	CV	
HUT	10.47	0.52	4.94	a	0.59	0.02	3.11	a	0.60	0.027	4.46	−22.80
NR/HUT	41.79	1.25	2.99	b	0.19	0.01	3.32	b	0.00		-	−40.79
HMB	4.95	0.17	3.34	a	0.54	0.02	3.11	a	0.01	0.001	4.79	−19.31
NR/HMB	42.64	1.08	2.54	b	0.34	0.01	1.60	b	0.00		-	−39.91
HA					38.68	0.89	2.30		0.18	0.02	11.11	−17.14

* Different letters indicate a significant difference at the 5% significance level.

3.1.2. TOC, IC, and Zeta Potential (ζ) of Clays and HA

Untreated clays exhibited high total organic carbon (TOC) content, while those activated with NaCl showed lower values (0.19% for HUT and 0.34% for HMB, Table 2). Inorganic carbon (IC) was only detectable in unactivated samples, with 0.6% for HUT and 0.01% for HMB. The decrease in TOC is attributed to the pretreatment with H_3PO_4, which degrades organic matter and removes carbonates and bicarbonates, promoting more efficient activation [61]. In contrast, HA presented a high TOC (38.68 $\pm$ 0.89%) and low IC (0.18 $\pm$ 0.02%), reflecting its high organic matter content and the minor presence of carbonate salts.

The zeta potential (ζ) is a key electrokinetic property of clays, reflecting the electrical potential at the solid–liquid interface associated with the movement of particles in aqueous suspension [21,62,63]. Clays generally have a negative surface charge. Natural HMB clay showed a ζ of −9.31 mV (Table 2), while activated clays exhibited significantly more negative values (−39.91 mV for activated HMB and −40.79 mV for activated HUT). The differences in ζ are attributed to particle size, degree of hydration, chemical nature, surface topography, and charge density, consistent with the smaller particle size observed. Activation with NaCl significantly increased the absolute value of ζ, due to the incorporation of Na^{+} into the diffuse electrical double layer and the presence of hydroxyl groups, which enhance cation adsorption. Absolute ζ values greater than 30 mV indicate high colloidal stability, associated with the weakening of Van der Waals forces and increased electrostatic

repulsion. Consequently, activated clays exhibit greater stability in aqueous media and superior cation exchange capacity and metal adsorption [21,63–66].

The ζ of HA presents a value of −17.14 mV, which indicates a good capacity for aggregation and formation of flocs in aqueous solutions. This favors the adsorption of metallic cations, since the result obtained indicates that the total charge of HA is negative. This fact is due to the presence of carboxyl, hydroxyl, and carbonyl groups that are not pulverized, which would allow it to hydrate easily [67,68].

3.1.3. Particle Size of Clays and HA

Natural HMB clay exhibited a trimodal particle size distribution, with dominant fractions of 839.5 nm (53.0%) and 239.8 nm (46.4%), while activated HMB showed greater homogeneity, with 97.4% of particles measuring 487.5 nm (Table 3). Natural HUT showed a bimodal particle size distribution, which shifted towards smaller sizes after activation. The reduction in particle size in the activated clays is attributed to treatment with H_3PO_4, which dissolves carbonates and oxides. This process generates amorphous silica, acidic centers, and new pores, improving adsorption sites [69,70].

Table 3. Particle size values.

Raw Materials and Composites	Peak	Size (nm)	%
HUT	1	169.1	14.2
	2	589.6	85.8
NR/HUT	1	194.4	11.4
	2	417.4	88.6
HMB	1	37.6	0.6
	2	239.8	46.4
	3	839.5	53.0
NR/HMB	1	65.0	2.6
	2	487.5	97.4
HA	1	43.4	4.2
	2	421.7	95.8

The particle size distribution for HA showed two peaks, 43.4 nm (4.2%) and 421.7 nm (95.8%). This behavior is attributed to the atomization process, which induces electrostatic and chemical interactions, favoring agglomeration. Furthermore, the solubilization of proteins, lipids, and carbohydrates generates particles with different molecular diameters [68,71].

3.1.4. XRD and DC Analysis of Clays and HA

The study of X-ray diffraction allows us to understand the structural arrangement and composition of materials, as well as the spatial arrangement of their atoms or molecules.

The diffractograms of the natural clays show a mineralogical composition dominated by montmorillonite, kaolinite, muscovite, illite, vermiculite, quartz, and chlorite [72,73]. After activation, the attenuation or disappearance of characteristic peaks was observed, particularly the basal peak of montmorillonite (~2θ = 6.2°) and, to a lesser extent, that of kaolinite (~2θ = 12.3°), while quartz remained the major phase. Activation with NaCl promotes the incorporation of Na^+ into the clay matrix, thereby increasing the cation exchange capacity by enriching the monovalent cation fraction. Consequently, the activated HMB and HUT clays exhibit significant improvements in their physicochemical properties, including increased cation exchange capacity, high colloidal stability, and modifications in the degree of crystallinity [74,75]. In particular, natural HMB and HUT show high crystal

order, with DC of 76.61 and 77.37% respectively (Figure 1a); after activation, NR/HMB retains ordered domains similar to the original clay, because its DC does not decrease considerably, while NR/HUT exhibits a marked reduction in the order of the structure with DC 48.87%.

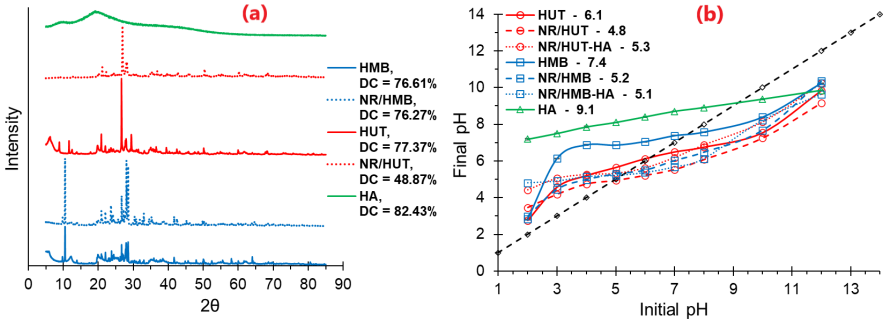


Figure 1. (**a**) XRD and DC of clays and HA; (**b**) zero charge point of clays, HA, and composites.

The hydrocolloid HA exhibited a type B diffraction pattern, with intense peaks around $2\theta \approx 20^\circ$ (Figure 1a), characteristic of the hexagonal double helix arrangement of structural water molecules, which is common in gums and hydrocolloids [75–77]. The determined degree of crystallinity (82.43%) indicates a highly permeable structure that favors hydration. However, this high crystallinity index should be interpreted as apparent crystallinity, linked to the supramolecular ordering induced by intermolecular interactions between organic functional groups, rather than as conventional mineral crystallinity. The presence of polysaccharides and proteins confers high chelation capacity, thermal stability, and a negative ζ, favoring flocculation and the adsorption of heavy metals, thus positioning HA as a functional hydrocolloid for water treatment applications.

3.1.5. Zero Charge Point Analysis

The zero charge point (ZCP) corresponds to the pH at which the surface of the material presents equivalent positive and negative charges [76,77]. Composites and activated clays show ZPC values around 5.1 (Figure 1b), indicating that at pH $\geq$ 5.1, their surfaces become negatively charged, favoring the attraction of metal cations [17,78,79]. In contrast, natural clays (HUT, HMB) and HA exhibit higher ZPC, associated with the high density of negative functional groups, mainly –OH in clays and $–COO^-$, –OH, and –CO in HA. The activation significantly reduces the ZPC, increasing the adsorption efficiency in acidic media, consistent with the species of As, Cd, Pb, and Zn. These conditions favor NR/HUT-HA and NR/HMB-HA composites' chemosorption mechanisms, including complexity, covalent coordination, hydrogen sources, and ionic exchange, resulting in selective and stable adsorption.

Since the pHZPC was reported to be around 5.1 for both composites, the adsorption study was carried out at pH 4.5 and 5.5, as the composite has both organic (HA) and inorganic (NR) duality. A pH of 4.5 was considered because NR activity would be predominant, and adsorption would mainly manifest itself through cation exchange in the activated clay sheets, resulting in clay–metal chelation. In contrast, at pH 5.5, the functional groups of HA would be deprotonated, increasing the negative charge and allowing metal–composite complexation. Therefore, studying both pH values allows us to determine whether adsorption is predominantly through ion exchange or surface complexation in the adsorption process, or both, as well as whether chemisorption or physisorption is predominant.

3.2. Multimetals Adsorption Capacity

The results obtained in adsorption tests in multimetallic systems demonstrate that natural clays HMB and HUT have an intrinsic capacity for the removal of heavy metals, with a clear preference for Pb^{2+} compared to As, Cd, and Zn (Table 4). This selectivity is mainly associated with physicochemical factors such as ionic radiation, energy, and hydration radiation, as well as the affinity of cations for superficial clay sites. Activation with NaCl significantly increased the removal efficiency in both clays, highlighting the key role of ionic replacement by Na^{+}, the improvement of the cation exchange capacity, and the modification of the ZCP, which favors the interaction with metallic species in slightly acidic media [61,75,76,80].

Table 4. Percentage and removal capacity of the multimetal system.

pH	Raw Materials and Composites	As (λ 193.76 nm)				Cd (λ 326.11 nm)				Pb (λ 216.99 nm)				Zn (λ 202.55 nm)			
		q_e	R (%)	±s	*	q_e	R (%)	±s	*	q_e	R (%)	±s	*	q_e	R (%)	±s	*
4.5	HMB	0.253	22.25	0.24	a	0.021	3.88	0.09	a	0.411	78.35	0.1	a	0.056	5.23	0.3	a
	NR/HMB	0.283	24.91	0.51	b	0.037	6.73	0.16	b	0.427	81.43	0.06	b	0.08	7.46	0.51	b
	HMB-HA	0.238	30.61	0.45	c	0.054	12.21	0.6	c	0.517	98.59	0.14	c	0.083	8.61	0.33	c
	NR/HMB-HA	0.252	32.32	0.51	d	0.063	14.16	0.42	d	0.522	99.51	0.17	d	0.099	10.31	0.4	d
	HUT	0.271	23.82	0.36	a	0.03	5.39	0.25	a	0.447	85.25	0.08	a	0.084	7.79	0.36	a
	NR/HUT	0.303	26.67	0.42	b	0.041	7.38	0.16	b	0.466	88.92	0.23	b	0.087	8.13	0.3	a
	HUT-HA	0.242	31.13	0.17	c	0.065	14.63	0.2	c	0.517	98.53	0.09	c	0.097	10.15	0.24	b
	NR/HUT-HA	0.258	33.12	0.2	d	0.075	16.91	0.46	d	0.522	99.52	0.01	d	0.125	13.07	0.4	c
5.5	HMB	0.281	24.76	0.41	a	0.086	15.68	0.52	a	0.419	79.88	0.19	a	0.088	8.17	0.51	a
	NR/HMB	0.305	26.87	0.47	b	0.044	7.92	0.34	c	0.429	81.72	0.19	b	0.102	9.51	0.3	b
	HMB-HA	0.245	31.52	0.26	c	0.063	14.36	0.31	b	0.519	98.9	0.16	c	0.101	10.57	0.28	c
	NR/HMB-HA	0.262	33.64	0.6	d	0.07	15.91	0.62	a	0.523	99.65	0.03	d	0.166	17.32	0.33	d
	HUT	0.306	26.95	0.24	a	0.04	7.22	0.48	a	0.449	85.55	0.28	a	0.102	9.55	0.5	a
	NR/HUT	0.324	28.55	0.23	b	0.064	11.64	0.89	b	0.47	89.66	0.32	b	0.111	10.36	0.3	a
	HUT-HA	0.246	31.64	0.34	c	0.069	15.7	0.42	c	0.519	98.93	0.05	c	0.121	12.65	0.42	b
	NR/HUT-HA	0.271	34.78	0.43	d	0.076	17.11	0.51	c	0.523	99.74	0.02	d	0.137	14.29	0.66	c
4.0	Cellulose/Chitin, 1000 mg/L, multimetal					0.32				0.33						[81]	
5.0	Cellulose/Citric acid, 2500 mg/L, single metal										94					[82]	
5.5	Tricarboxylic cellulose, 1000 mg/L, multimetal									0.47						[83]	
5.5	Activated cellulose, 1000 mg/L, multimetal					0.58				0.55				0.4		[29]	
7.0	Cellulose/Fe_3O_4, 1666 mg/L, multimetal					0.3				0.56	90					[84]	
4.0	Rice husk/Fe_2O_3, 300 mg/L, multimetal	0.13														[85]	
5.0	Cellulose/TSC, 70 mg/L, multimetal						≈100				≈100					[86]	
6.0	Activated clay, 2000 mg/L, single metal										80					[87]	

Table 4. *Cont.*

pH	Raw Materials and Composites	As (λ 193.76 nm)				Cd (λ 326.11 nm)				Pb (λ 216.99 nm)				Zn (λ 202.55 nm)			
		q_e	R (%)	±s	*	q_e	R (%)	±s	*	q_e	R (%)	±s	*	q_e	R (%)	±s	*
4.5	Clay/Fe_2O_3/ Activated charcoal, 2000 mg/L, multimetal	0.07				0.37				0.36						[88]	
5.5	Clay/HCl, 2000 mg/L, single metal										98					[80]	
7.5	Activated charcoal, 10,000 mg/L, multimetal					0.43				0.43				0.92		[89]	
5.0	Activated charcoal, 20,000 mg/L, multimetal					0.34				0.2				1.48		[90]	

λ is the wavelength, R is the average percentage of adsorption for 3 replicates, S is the standard deviation, and q_e is the equilibrium adsorption capacity (mmol/g). * Different letters indicate a significant difference at the 5% significance level, assessed using Tukey's test at a significance level of 0.05.

However, the most outstanding performance was observed in the NR/HMB-HA and NR/HUT-HA composites. These composites achieved Pb^{2+} removal efficiencies exceeding 99.5% (0.522 mmol/g) at pH 4.5 and up to 99.74% (0.523 mmol/g) at pH 5.5, significantly outperforming both individual clays and various adsorbents reported in the literature, including modified cellulosic materials, activated carbons, and ion exchange resins, as shown in Table 4.

The superior performance of the composites is explained by a marked synergistic effect between the inorganic and biological components. Activated clay provides a layered structure with a high surface area, larger pore volume, and high density of exchangeable sites, while the HA introduces an organic matrix rich in functional groups (–COO^-, –OH, and –NH) capable of participating in chemisorption, complexation, and hydrogen bonding mechanisms. This combination increases the density and accessibility of the active sites, even under the ionic competition typical of multimetal systems [91–96].

Thus, the high efficiency observed at slightly acidic pH is particularly relevant for the remediation of industrial effluents and mining leachates, where metal precipitation is limited. Taken together, the results confirm that clay–HA composites are highly efficient, selective, and environmentally sustainable adsorbents, positioning them as a promising alternative for advanced heavy metal removal in complex aqueous systems. Although we believe that other controllable and uncontrollable parameters (noise) could negatively influence adsorption capacity, in practical cases, competition from dissolved ions and the pH of the aqueous medium or water body are usually the main challenges to overcome when applying new adsorbents.

3.3. FTIR and SEM Analysis of Post-Adsorption Composites

FTIR spectroscopy characterization of the NR/HMB-HA and NR/HUT-HA composites, before and after adsorption in multimetallic aqueous solutions, allows for the clear identification of the functional groups responsible for the interaction with metal ions and a better understanding of the adsorption mechanisms involved. In the initial spectra, both composites exhibit intense bands around 3430–3425 cm^{-1} and 2930 cm^{-1} (Figure 2), associated with the stretching of –OH, –NH, –C–O–, and –C=O groups. These signals are primarily attributed to the powdered Nostoc hydrocolloid (HA), as well as to the structural hydroxyl groups of the activated clay.

Following adsorption at pH 4.5 and 5.5, a significant decrease in intensity and slight shifts in these bands were observed, demonstrating the direct involvement of these functional groups in the complexation of Pb^{2+}, Cd^{2+}, Zn^{2+}, and As^{3+}. In particular, the variations in the 530–690 cm^{-1} regions indicate interactions between the metals and the Al–O–Si and Si–O bonds of the activated clay, located primarily on the octahedral surface. This behavior confirms that the inorganic matrix actively contributes to the retention of metal cations through ion exchange and surface complexation mechanisms [61,97].

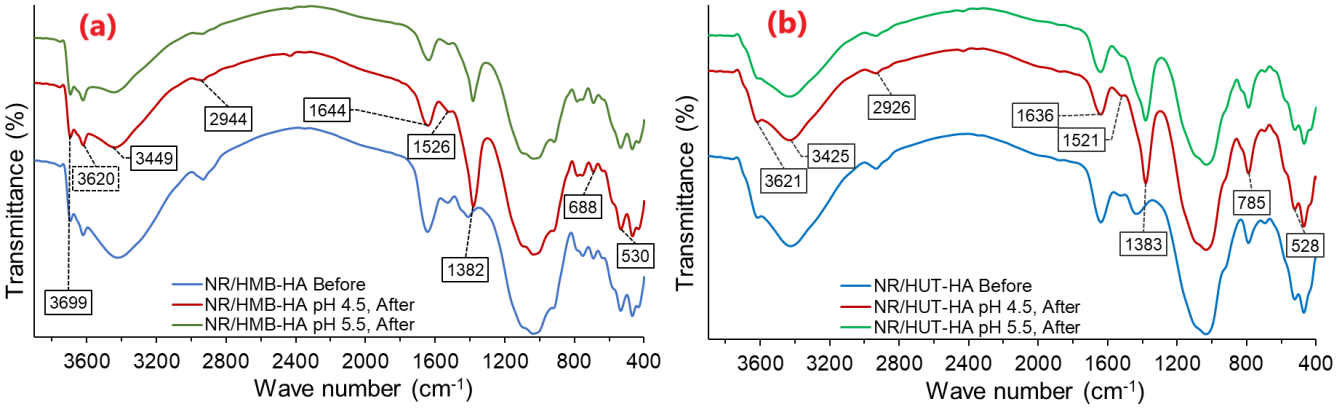


Figure 2. FTIR spectra before and after adsorption, (**a**) NR/HMB-HA composite, (**b**) NR/HUT-HA composite.

Furthermore, the disappearance of bands around 1430 cm^{-1} and the emergence of new, intense signals near 1380 cm^{-1} constitute clear evidence of metal complex formation, especially with Pb^{2+}. Similarly, the decrease in intensity around 1520 cm^{-1}, attributed to –NH, C=O, and –C(=O)–NH stretching of HA, reveals the involvement of oxygen and nitrogen donor atoms in the coordination of Cd^{2+}, Zn^{2+}, and Pb^{2+}. The reduction in the band near 1630 cm^{-1} reinforces this behavior, indicating the action of the –OH, –C=O, and –CN groups of the hydrocolloid and clay during the adsorption process, mediated by electrostatic and Van der Waals forces [9,98,99].

Regarding the spectra around 3449 and 3425 cm^{-1}, for the NR/HMB-HA and NR/HUT-HA composites, respectively, they showed a considerable decrease in intensity, which demonstrates the ability to remove heavy metals, due to the synergistic effect of the –OH functional groups of the octahedral sheet in the activated clay, and the –NH and –OH groups of the HA [99,100]. Furthermore, the high frequency bands at 3620–3690 cm^{-1} show a slight decrease in intensity after adsorption, confirming the complexation of two groups –Al–OH and –Si–OH in activated clay. Overall, the FTIR results, corroborated by morphological analyses by SEM (Figure 3), demonstrate a pronounced synergistic effect between the biological and inorganic components of the two composites. This synergy increases the density and diversity of active sites [75,80], favors the formation of stable metal complexes, and explains the high efficiency of the NR/HMB-HA and NR/HUT-HA composites in the removal of heavy metals in multimetallic aqueous systems under different pH conditions.

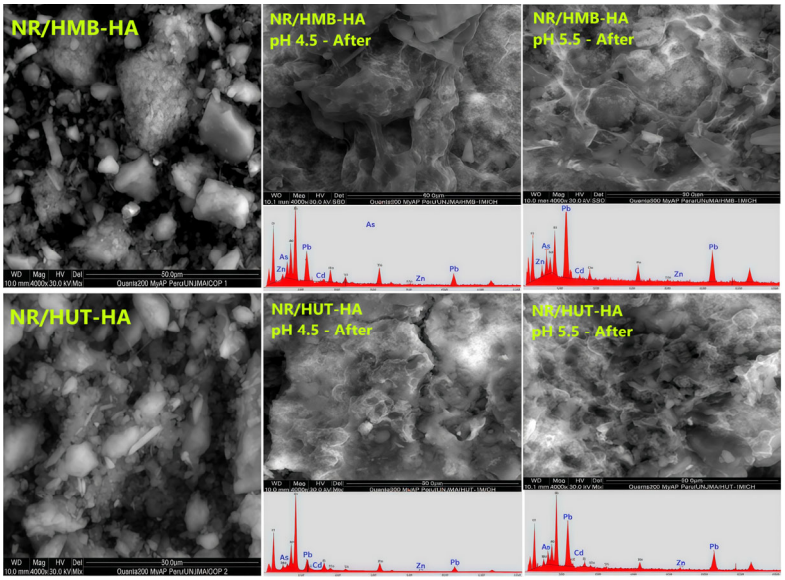


Figure 3. SEM micrographs before and after the adsorption process.

3.4. Multimetal Adsorption Kinetics

The kinetic study of the adsorption of NR/HMB-HA and NR/HUT-HA composites allows us to quantify the speed of the process, identify the controlling steps, and evaluate the physicochemical nature of the metal–adsorbent interaction in multimetallic systems [101,102]. These adsorption mechanisms can be explained through four processes: (i) migration towards the surface, (ii) diffusion within the monolayer, (iii) intraparticle or pore diffusion, and (iv) sorption at interior sites; phases for (i) and (iii) occur spontaneously due to the availability of metals near the surface. Phases for (ii) and (iv) generally control the adsorption rate, and the intraparticle model allows us to explain this phenomenon [95,103].

Experimentally, rapid adsorption was observed in the first 10–15 min (Figure 4), followed by a slower stage until reaching equilibrium within 90 min, typical behavior of materials with a high density of active sites and high colloidal stability, associated with highly negative values of ζ. During longer periods, adsorption is very slow and occurs mainly within the pores; therefore, processes (iii) and (iv) would be observed. This behavior is common in clay materials subjected to the adsorption of Pb^{2+}, Cd^{2+}, Zn^{2+} [8,87,100].

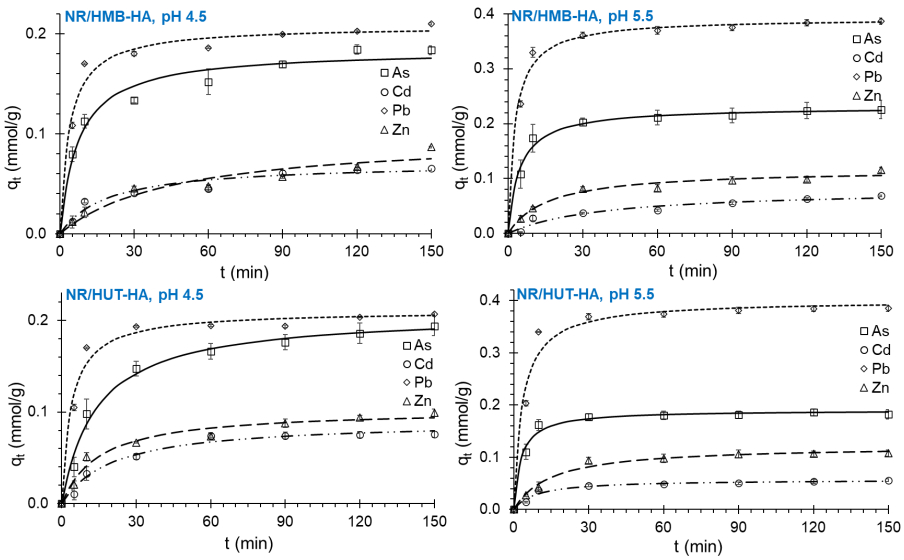


Figure 4. Multimetal adsorption kinetics evaluated through the PSO model.

The adjustment of experimental data to the PSO model shows the largest correlation coefficients ($R^2 > 0.98$) and the smallest statistical errors (*ARE* and χ^2) in comparison with the other models (Table 5), which validates the model, indicating that the adsorption is dominated by chemosorption [8,92]. The kinetic constants k_2 presented the highest values for Pb^{2+} (Table 6), followed by As^{3+}, Zn^{2+}, and Cd^{2+}, showing a higher pole fixation speed. This tendency is directly related to the greater ionic radius and lower hydration energy of Pb^{2+}, which favor the formation of stable complexes with the functional groups of the composite.

The PFO model adequately describes the initial stage of the process; however, it presented R^2 values lower than PSO, which indicates that this model does not completely represent the global adsorption mechanism. This confirms that metal retention is not governed solely by physical processes of superficial diffusion, but involves specific chemical interactions.

Table 5. Kinetic model fitting statistics.

Metallic Ion	Model	NR/HMB-HA						NR/HUT-HA					
		pH 4.5			pH 5.5			pH 4.5			pH 5.5		
		R^2	X^2	*ARE*	X^2	R^2	*ARE*	R^2	X^2	*ARE*	X^2	R^2	*ARE*
As	PFO	0.921	0.011	10.539	0.998	0.002	4.026	0.956	0.006	9.553	0.999	0.000	2.056
	PSO	0.961	0.004	6.844	0.999	0.003	4.396	0.967	0.006	9.713	0.999	0.003	4.176
	Elovich	0.954	0.010	7.173	0.994	0.044	14.457	0.961	0.010	15.396	0.999	0.072	19.614
	IPD	0.954	0.017	11.516	0.821	0.045	14.563	0.923	0.057	21.662	0.801	0.045	16.584
	CD	0.781	0.005	7.462	0.857	0.007	7.145	0.812	0.097	24.196	0.901	0.003	5.498
Cd	PFO	0.981	0.009	14.462	0.981	0.018	41.287	0.996	0.003	12.138	0.997	0.003	13.118
	PSO	0.994	0.005	13.400	0.986	0.013	48.921	0.997	0.004	16.157	0.998	0.004	13.454
	Elovich	0.992	0.005	20.409	0.981	0.016	110.616	0.983	0.009	32.238	0.998	0.006	16.787
	IPD	0.981	0.007	17.973	0.991	0.014	67.559	0.907	0.021	30.353	0.879	0.014	22.761
	CD	0.811	0.011	28.147	0.805	0.026	138.069	0.812	0.048	45.937	0.875	0.008	21.115
Pb	PFO	0.993	0.004	5.798	0.998	0.001	2.178	0.990	0.002	4.275	0.999	0.004	3.932
	PSO	0.999	0.004	5.505	0.999	0.003	2.928	0.991	0.004	5.837	0.999	0.011	6.173
	Elovich	0.999	0.055	15.638	0.999	0.145	18.995	0.983	0.059	17.153	0.993	0.131	17.851
	IPD	0.837	0.042	14.403	0.787	0.085	16.364	0.824	0.121	15.540	0.782	0.102	15.606
	CD	0.871	0.007	8.360	0.887	0.005	4.729	0.873	0.082	7.280	0.879	0.014	7.784
Zn	PFO	0.934	0.013	23.775	0.967	0.005	8.850	0.981	0.008	12.459	0.996	0.001	3.944
	PSO	0.961	0.007	17.019	0.989	0.003	6.491	0.997	0.005	11.163	0.999	0.003	8.073
	Elovich	0.961	0.054	33.679	0.987	0.006	13.225	0.996	0.004	14.549	0.991	0.008	18.094
	IPD	0.967	0.005	13.398	0.935	0.010	12.273	0.961	0.024	17.015	0.821	0.021	17.358
	CD	0.781	0.024	42.688	0.812	0.014	21.044	0.807	0.048	23.265	0.873	0.018	26.421

Elovich's model provided key information about the heterogeneity of the adsorbent surface. The high values of the parameter α (initial adsorption speed) reflect the rapid occupation of the most energetic active sites, while the relatively low values of β indicate a progressive decrease in the speed as the surface coverage increases. This model describes particularly good Pb^{2+} adsorption, suggesting a strong interaction with $–COO^-$, –OH, and –NH groups of HA, as well as with the Al–O–Si and Si–O bonds of activated clay.

The intraparticle diffusion model presented relatively low R^2 values, even higher than 0.70, which indicates an acceptable model. In this sense, it suggests that intraparticle diffusion participates partially in the adsorption process. In this context, the intraparticle velocity constants (k_{id}) were greater for Pb^{2+}, followed by the order $As^{3+} > Zn^{2+} > Cd^{2+}$, which shows that migration occurs on the surface of the adsorbent and diffusion within the pores occurs faster for Pb^{2+} and As^{3+}. Therefore, the surface diffusion processes and

the sorption in the internal sites of the composite constitute the controlling factors of the adsorption speed, which is directly related to the hydration radiation.

Table 6. Kinetic model parameters for multimetal systems.

Composite	Model	Parameters	pH 4.5				pH 5.5			
			As	Cd	Pb	Zn	As	Cd	Pb	Zn
NR/HMB-HA	PFO	q_e (mmol/g)	0.167	0.061	0.197	0.079	0.217	0.066	0.376	0.100
		k (min^{-1})	0.109	0.043	0.173	0.020	0.147	0.025	0.202	0.055
	PSO	q_e (mmol/g)	0.184	0.071	0.208	0.098	0.231	0.081	0.392	0.117
		k_2 (g/mmol.min)	0.746	0.741	1.295	0.219	0.943	0.330	0.915	0.532
	Elovich	α (g/mmol.min)	0.042	0.011	0.060	21.675	0.061	0.010	0.126	11.285
		β (g/mmol)	26.141	79.643	0.000	71.086	19.896	83.499	0.020	46.800
	Intraparticle diffusion	k_{id} (mmol/g.$min^{1/2}$)	0.013	0.005	0.013	0.007	0.015	0.006	0.024	0.009
		C (mmol/g)	0.042	0.006	0.071	0.000	0.072	0.001	0.152	0.012
	Crank diffusion	q_e (mmolg/g)	0.169	0.059	0.191	0.065	0.211	0.057	0.365	0.097
		$D_s \times 10^{-11}$ (m^2/s)	3.207	1.959	9.015	1.550	7.133	1.692	11.274	2.332
NR/HUT-HA	PFO	q_e (mmol/g)	0.182	0.076	0.199	0.089	0.182	0.052	0.381	0.106
		k (min^{-1})	0.062	0.044	0.166	0.058	0.197	0.092	0.176	0.058
	PSO	q_e (mmol/g)	0.208	0.090	0.210	0.103	0.190	0.058	0.401	0.122
		k_2 (g/mmol.min)	0.344	0.546	1.258	0.648	1.851	1.950	0.724	0.551
	Elovich	α (g/mmol.min)	0.036	0.011	0.055	21.522	0.060	0.011	0.117	11.220
		β (g/mmol)	25.563	64.122	0.016	52.108	23.358	86.098	0.020	44.129
	Intraparticle diffusion	k_{id} (mmol/g.$min^{1/2}$)	0.016	0.007	0.013	0.008	0.011	0.004	0.025	0.009
		C (mmol/g)	0.026	0.006	0.073	0.012	0.074	0.011	0.146	0.015
	Crank diffusion	q_e (mmolg/g)	0.175	0.071	0.193	0.088	0.177	0.050	0.369	0.101
		$D_s \times 10^{-11}$ (m^2/s)	3.886	2.435	8.823	2.269	15.506	4.011	9.712	2.946

On the other hand, the constant C, associated with the thickness of the limit layer, presented higher values for Pb^{2+} and As^{3+}, while for Zn^{2+} and Cd^{2+} they were significantly lower. When C is distinct from zero, it is confirmed that the adsorption process is complex and is governed by more than one diffusive resistance, ruling out intraparticle diffusion as the only controlling step. Even though the C and k_{id} values obtained are lower in comparison with other advanced adsorbent materials such as metal oxides, magnetic composites, carbon nanotubes, and biomass residues, among others, these results indicate that the slow diffusion of metallic ions within the pores of the studied composites constitutes a relevant limiting stage of the global adsorption process.

The Crank diffusion model is applied to porous materials, allowing us to determine the rate at which the adsorbate diffuses within the adsorbent. It was observed that the diffusivity constant (D_e) was higher for treatments at pH 5.5 in both composites. This is closely related to the speciation of ionized metals; however, the diffusion process in the composites is greater for Pb^{2+}, reaching values of 9.712×10^{-11} m^2/s in NR/HUT-HA and 11.274×10^{-11} m^2/s for NR/HMB-HA at pH 5.5. Although this model reported R^2 values between 0.781 and 0.901, it suggests that this model relatively explains the adsorption process in multimetal systems; however, the De parameter may provide information on the design of adsorption systems.

In both composites, q_e and surface diffusivity (D_s) were reported to follow the order Pb > As > Zn > Cd. Although it was slightly higher for the NR/HUT-HA composite, suggesting that despite the compositional difference due to the clay types, HA conditions the final adsorption of metal ions, so the union of a biological and inorganic material could present better adsorption qualities.

3.5. Adsorption Isotherms

Adsorption equilibrium studies demonstrated that composites reached equilibrium in approximately 90 min, demonstrating fast kinetics at low metal concentrations in multimetallic systems. At constant temperature, adsorption showed a marked preference for Pb^{2+}, while As^{3+}, Cd^{2+}, and Zn^{2+} reached saturation more quickly at high concentrations (Figure 5). This behavior is mainly associated with ionic competence, whereby ions with a greater ionic radius and lower hydration energy present a high affinity for the active sites of the adsorbent [76,104]. However, additional factors such as the type of adsorbent, the degree of activation, and the agitation of the system also significantly influence the process [93,104].

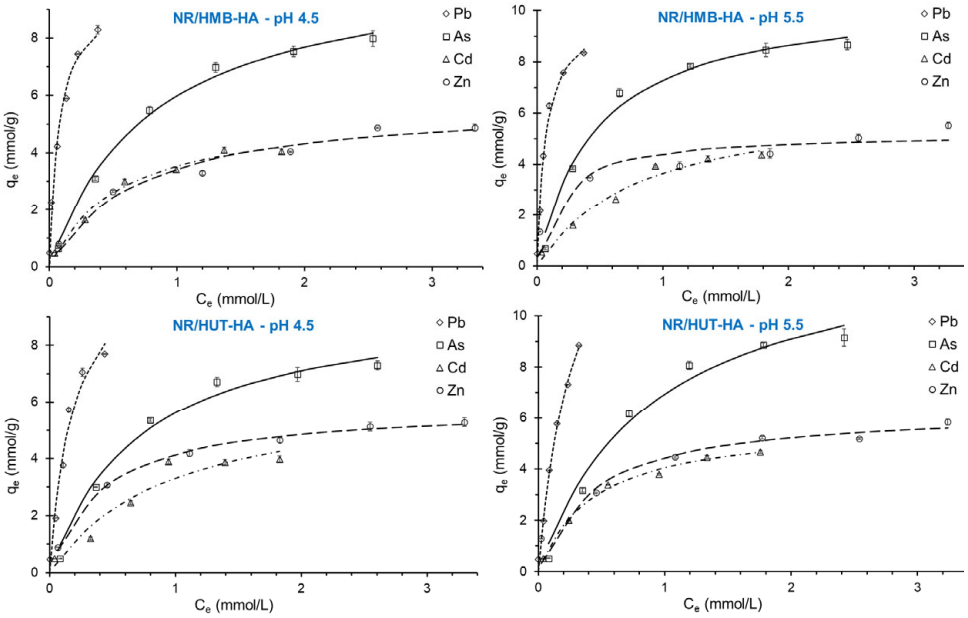


Figure 5. Multimetal adsorption isotherms evaluated through the Langmuir model.

The comparison between unimetallic and multimetallic systems showed a clear competitive effect. In unimetallic systems, a significant increase in adsorption capacity was observed, particularly for Cd^{2+} and Zn^{2+}, confirming that in multimetallic systems these ions are disadvantaged compared to Pb^{2+}. Furthermore, Pb^{2+} maintains high removal efficiencies in both systems, reaching values above 99% for both composites (Table 7), which confirms its high affinity for the available active sites. Therefore, ions exhibit competition in multimetallic systems, which is a characteristic behavior [20,80,87,105,106].

The Langmuir model adequately described monolayer adsorption, showing high values of maximum adsorption capacity (q_{max}) for Pb^{2+} and As^{3+}, especially at pH 5.5 (Table 8). Although the q_{max} values are higher than those reported in the literature [87,103,107], this is due to the activation of the clays and the atomized nostoc (HA), which have a nanoparticle size and low ζ, which gives them suspension stability, allowing them to come into contact with the multimetal solution. This increase in pH is attributed to the ZCP of the composites, as above pH 5 the surface presents a greater density of negative charges, favoring the electrostatic attraction of metal cations. The K_L parameter indicates a high binding energy for Pb^{2+}, highlighting the NR/HMB-HA composite with values of up to 14.63 L/mmol, which confirms a high chemical affinity between the metal and the adsorbent [76,108].

Table 7. Comparison of removal (%) for unimetal and multimetal isotherms.

pH	Composite	As					Cd					Pb					Zn			
		C_0	U		M		C_0	U		M		C_0	U		M		C_0	U		M	
			R	±S	R	±S		R	±S	R	±S		R	±S	R	±S		R	±S	R	±S
4.5	NR/HMB-HA	0.13	56.77	0.80	48.50	0.44	0.09	75.60	0.20	54.77	0.51	0.05	99.10	0.10	98.33	0.15	0.15	75.33	0.93	52.60	1.21
		0.67	52.70	0.74	46.45	0.76	0.44	50.85	0.26	37.08	1.21	0.24	95.08	0.13	94.00	0.17	0.76	46.10	0.38	34.73	0.53
		1.33	44.29	0.92	41.17	0.95	0.89	38.74	0.72	33.78	0.79	0.48	90.58	0.07	87.47	1.39	1.53	32.04	0.31	21.61	0.40
		2.00	37.37	0.82	34.87	0.83	1.33	31.69	0.78	25.59	0.61	0.72	82.66	0.07	81.43	0.10	2.29	26.11	0.13	17.63	0.08
		2.67	31.25	0.61	28.24	0.67	1.78	30.63	0.65	23.02	0.57	0.97	78.79	0.09	77.09	0.13	3.06	26.04	0.16	15.94	0.08
		3.33	26.43	0.80	23.93	0.83	2.22	24.84	0.30	18.21	0.33	1.21	70.40	1.28	68.64	1.29	3.82	24.25	0.29	12.77	0.34
	NR/HUT-HA	0.13	52.03	0.25	37.73	0.51	0.09	75.53	0.95	56.33	0.58	0.05	98.93	0.06	98.13	0.40	0.15	80.10	0.78	58.37	0.50
		0.67	51.63	0.35	45.07	0.25	0.44	46.27	1.06	27.00	1.32	0.24	84.57	0.10	79.42	0.12	0.76	51.13	0.93	40.27	1.01
		1.33	43.45	0.34	40.17	0.38	0.89	37.05	0.46	27.58	0.76	0.48	83.32	0.09	78.01	1.44	1.53	37.60	0.29	27.42	0.76
		2.00	35.76	0.69	33.53	0.83	1.33	35.16	0.76	29.20	0.60	0.72	79.55	1.18	79.07	1.15	2.29	28.55	0.43	20.27	0.42
		2.67	29.37	0.71	26.17	0.95	1.78	29.20	0.57	21.75	0.50	0.97	75.35	0.81	73.01	1.44	3.06	26.60	0.47	16.75	0.50
		3.33	24.49	0.55	21.87	0.50	2.22	24.36	0.48	17.87	0.50	1.21	67.42	0.13	63.75	0.16	3.82	25.08	0.43	13.80	0.40
5.5	NR/HMB-HA	0.13	63.37	0.45	51.43	2.53	0.09	80.30	1.05	61.10	0.89	0.05	99.23	0.15	98.13	0.25	0.15	95.60	0.30	87.87	0.58
		0.67	61.88	0.39	57.78	0.60	0.44	55.68	0.40	35.75	0.76	0.24	92.47	0.13	89.60	2.00	0.76	56.28	0.29	45.42	0.15
		1.33	53.05	0.78	50.92	1.26	0.89	44.33	0.29	29.54	0.13	0.48	91.92	0.08	89.72	1.51	1.53	38.14	0.21	25.78	1.00
		2.00	41.11	0.15	39.21	0.23	1.33	35.41	0.22	29.45	0.33	0.72	88.31	0.42	86.77	1.40	2.29	27.55	0.81	19.27	0.81
		2.67	34.47	0.89	31.75	1.00	1.78	31.14	0.79	23.69	0.58	0.97	82.07	0.09	78.40	0.17	3.06	26.32	0.53	16.47	0.45
		3.33	27.91	0.57	26.00	0.60	2.22	26.13	0.44	19.63	0.50	1.21	72.03	0.16	69.13	0.26	3.82	25.72	0.37	14.44	0.31
	NR/HUT-HA	0.13	55.20	0.75	39.20	1.00	0.09	78.43	0.61	57.10	0.87	0.05	99.07	0.15	98.23	0.15	0.15	92.57	0.96	84.83	0.61
		0.67	52.55	0.10	47.43	1.04	0.44	54.95	0.70	45.35	0.87	0.24	85.28	0.15	82.10	0.40	0.76	51.12	0.23	40.25	0.35
		1.33	48.74	0.86	46.25	0.90	0.89	42.75	0.28	37.95	0.20	0.48	82.68	0.10	81.93	0.14	1.53	42.12	0.31	29.18	0.29
		2.00	42.30	0.77	40.31	0.81	1.33	34.35	0.27	28.39	0.23	0.72	80.22	0.50	79.75	0.50	2.29	31.03	0.18	22.75	0.23
		2.67	35.77	0.29	33.28	0.25	1.78	32.48	0.33	25.03	0.40	0.97	77.40	0.18	75.81	0.16	3.06	26.82	0.09	16.97	0.11
		3.33	28.79	0.66	27.47	1.01	2.22	27.48	0.28	20.99	0.22	1.21	75.21	0.17	73.34	0.20	3.82	26.55	0.25	15.27	0.31

C_0 is the initial concentration (mmol/L); R is the average percentage of adsorption for n = 3; S is the standard deviation; U indicates unimetal; and M indicates multimetal.

Table 8. Parameters of isotherm models in a multimetal system.

pH	Composite	Metal	Langmuir		Freundlich			Redlich–Peterson			Temkin	
			q_{max}	K_L	K_f	1/n	n	k_R	a_R	g	b_t	A_t
4.5	NR/HMB-HA	As	10.706	1.267	5.502	0.481	2.081	10.119	0.632	1.360	1140.518	16.860
		Pb	9.655	13.98	12.683	0.393	2.545	492.93	41.492	0.701	1912.576	941.12
		Cd	5.462	1.821	3.345	0.460	2.175	7.769	1.153	1.252	2435.631	32.040
		Zn	5.794	1.465	3.149	0.402	2.484	21.842	5.642	0.730	2263.650	25.582
	NR/HUT-HA	As	9.673	1.385	5.122	0.466	2.144	9.126	0.533	1.532	1165.449	14.556
		Pb	11.535	5.276	12.552	0.503	1.989	41.081	6.876	1.971	2149.958	759.62
		Cd	6.503	1.039	3.167	0.541	1.847	4.259	0.165	2.991	2456.684	27.843
		Zn	5.864	2.400	3.706	0.344	2.910	18.26	3.506	0.909	2160.616	34.685
5.5	NR/HMB-HA	As	10.613	2.190	6.612	0.407	2.460	16.80	1.188	1.300	1057.168	21.755
		Pb	10.061	14.63	13.125	0.387	2.587	114.18	13.895	1.221	1795.829	797.00
		Cd	6.629	1.223	3.489	0.514	1.946	5.341	0.389	1.917	2373.685	33.568
		Zn	5.223	5.193	3.966	0.255	3.928	555.73	137.66	0.764	3254.014	274.23
	NR/HUT-HA	As	13.226	1.103	6.393	0.519	1.925	9.917	0.344	1.771	887.305	12.901
		Pb	16.696	3.467	18.715	0.646	1.547	55.08	3.553	1.101	1927.913	732.91
		Cd	5.813	2.279	3.842	0.440	2.272	14.083	2.500	0.962	2190.540	35.250
		Zn	6.357	2.298	4.138	0.299	3.349	424.41	100.69	0.718	2695.288	137.12

q_{max} (mmol/g); K_L (L/mmol); K_f (mmol$^{1-1/n}$/L^n); 1/n, n, k_R (L/g); a_R (L/mmol)^g; g, b_t (J/Mol); A_t (L/mmol) are the parameters of isothermal models.

The Freundlich model showed a heterogeneous surface of composites, with values of 1/n less than 1, which indicates a high initial affinity and a rapid saturation of the most energetic sites [109–112]. Values of n between 1 and 10 confirm that adsorption is favorable for all metals studied, with a greater preference for Pb^{2+}. These results are consistent with

the heterogeneous nature of the material, resulting from the combination of activated clay and hydrocolloid of biological origin.

The values of the separation factor R_L, derived from the Langmuir model, were between 0 and 1 for all systems evaluated, confirming that the adsorption process is favorable. For Pb^{2+}, lower R_L values were obtained (Table 9), especially in NR/HMB-HA, which suggests irreversible adsorption and strong metal fixation, associated with chemisorption processes and intraparticular diffusion in internal sites of the composite [9,88,95,103].

On the other hand, the Redlich–Peterson empirical model, called the "three-parameter equation", has parameters that lack physicochemical and thermodynamic explanations [113–115]. High values of the K_R parameter indicate a greater affinity between the metal ions and the composite, being higher for Pb and Zn (Table 8). Whereas, the a_R parameter is related to the heterogeneity of the composite surface [113,115]. a_R values close to unity indicate a more homogeneous surface, while values further from unity indicate heterogeneity. It was observed that, in most cases, a_R is greater than 1.0, which confirms the heterogeneity of the composites studied; that is, the composites studied exhibit a heterogeneous surface. However, no correlation was observed between the K_R, a_R, and g parameters and the Langmuir and Freundlich model parameters.

Table 9. RL values for adsorption evaluated through the Langmuir model.

Composite	pH 4.5				pH 5.5			
	As	Pb	Cd	Zn	As	Pb	Cd	Zn
NR/HMB-HA	0.8554	0.5971	0.8606	0.8170	0.7740	0.5862	0.9019	0.5574
	0.5420	0.2286	0.5525	0.4716	0.4065	0.2208	0.6477	0.2012
	0.3718	0.1291	0.3817	0.3086	0.2551	0.1241	0.4789	0.1119
	0.2829	0.0899	0.2916	0.2293	0.1858	0.0863	0.3799	0.0775
	0.2283	0.0690	0.2359	0.1824	0.1462	0.0661	0.3149	0.0592
	0.1914	0.0560	0.1981	0.1515	0.1205	0.0536	0.2688	0.0480
NR/HUT-HA	0.8441	0.7970	0.9154	0.7315	0.8718	0.8567	0.8314	0.7400
	0.5199	0.4399	0.6839	0.3527	0.5762	0.5445	0.4966	0.3627
	0.3513	0.2820	0.5196	0.2141	0.4047	0.3741	0.3303	0.2215
	0.2652	0.2075	0.4190	0.1537	0.3119	0.2849	0.2475	0.1595
	0.2131	0.1641	0.3510	0.1199	0.2537	0.2301	0.1978	0.1246
	0.1780	0.1358	0.3020	0.0983	0.2138	0.1929	0.1648	0.1022

Regarding the Temkin model, the b_T parameter is related to the heat of adsorption, while A_T corresponds to the maximum binding energy. These parameters allow us to establish the interactions between the ionic metals and the adsorbent, consistent with chemisorption [116,117]. It was observed that A_T was higher for Pb^{2+} (Table 8), suggesting that the binding forces are stronger for this ion, agreeing with the Langmuir K_L parameter [52]. In addition, b_T is lower for As and Pb in both composites, suggesting that these ions require less energy to establish bonds with the active sites of the adsorbent [118,119].

The models studied reported R^2 values between 0.7152 and 0.9994 (Table 10); these results suggest a good fit of the experimental data to the models. On the other hand, the calculation of X^2, *ARE*, *HYBRID*, and *MPSD* is based on the difference between the experimental value and the value of q_e reported by the model; therefore, it is desirable to expect the values to be as low as possible [51–53]. It was observed that X^2 ranged from 0.0025 to 5.2038, while *ARE* ranged from 0.8898 to 69.0453, *HYBRID* from 1.6207 to 103.5680, and *MPSD* from 0.0614 to 1.8022.

A predominant order of Pb > Zn > Cd > As is observed (Table 11), although this does not necessarily correlate with the removal percentage. In competitive affinity, metal–ligand bonds are established with the active sites, forming strong internal complexes with the carboxyl and hydroxyl groups. This results in Pb^{2+} having a higher k_{Li} value due to its lower hydration energy, while Zn^{2+} has a smaller hydration radius than Cd^{2+}, allowing it to diffuse more rapidly across the adsorbent surface and establish more stable bonds. As, in the studied pH range, ionizes to $H_2AsO_4^-$, resulting in low k_{Li} values. Another aspect to consider is that k_{Li} decreases for metals at pH 5.5. This is due to increased competition for negatively charged active sites (above pH_{ZCP}), favoring the formation of metal–composite complexes.

Based on statistical criteria, the Langmuir model best fits the experimental data (although the others also show good results across statistical criteria), allowing us to assume that multimetal adsorption occurs mainly in homogeneous sites and at the monolayer level, with high q_{max} and high affinity (k_L), primarily for Pb^{2+}, increasing significantly at pH 5.5 due to the deprotonation of the composite's functional groups, resulting in favorable adsorption ($0 < R_L < 1$). Therefore, the statistical analysis supports the metal–composite chemical complexation mechanisms in the adsorption process.

Table 10. Statistics for the adjustment of isotherm models.

Metal Ion	Model	R^2	X^2	*ARE*	*HYBRID*	*MPSD*	R^2	X^2	*ARE*	*HYBRID*	*MPSD*
		NR/HMB-HA, pH 4.5					**NR/HMB-HA, pH 5.5**				
AS	Langmuir	0.994	0.092	8.392	12.588	0.253	0.984	0.370	18.388	27.582	0.455
	Freundlich	0.949	0.722	28.733	43.099	0.724	0.901	1.435	42.760	64.140	1.113
	Redlich–P.	0.999	0.006	1.752	3.504	0.094	0.995	0.146	10.367	20.735	0.300
	Temkin	0.981	0.165	13.884	20.827	0.450	0.982	0.138	7.216	10.825	0.477
Cd	Langmuir	0.985	0.085	8.749	13.124	0.195	0.973	0.361	13.941	20.911	0.291
	Freundlich	0.956	0.224	16.509	24.763	0.336	0.959	0.163	9.738	14.608	0.357
	Redlich–P.	0.988	0.138	9.893	19.787	0.207	0.980	0.741	14.911	29.821	0.289
	Temkin	0.956	0.163	15.403	23.104	0.337	0.903	0.380	26.197	39.296	0.547
Pb	Langmuir	0.982	1.552	20.225	30.337	0.448	0.987	1.040	18.029	27.043	0.392
	Freundlich	0.990	0.168	13.537	20.306	0.335	0.944	0.756	27.306	40.958	0.824
	Redlich–P.	0.995	0.118	7.839	15.678	0.276	0.993	1.402	17.314	34.628	0.348
	Temkin	0.917	0.662	44.387	66.581	0.973	0.879	1.112	53.377	80.066	1.209
Zn	Langmuir	0.967	0.200	10.537	15.806	0.314	0.859	1.866	17.207	25.811	0.620
	Freundlich	0.976	0.138	9.996	14.994	0.272	0.982	0.055	4.540	6.810	0.220
	Redlich–P.	0.985	0.053	5.194	10.389	0.248	0.983	0.044	3.696	7.392	0.246
	Temkin	0.972	0.078	7.481	11.221	0.289	0.903	0.084	6.078	9.117	0.320
		NR/HUT-HA, pH 4.5					**NR/HUT-HA, pH 5.5**				
AS	Langmuir	0.982	0.322	20.612	30.917	0.409	0.980	0.448	23.778	35.667	0.553
	Freundlich	0.916	1.080	43.798	65.697	0.875	0.926	1.298	48.007	72.010	1.058
	Redlich–P.	0.997	0.089	9.247	18.495	0.199	0.997	0.112	10.588	21.177	0.235
	Temkin	0.982	0.135	9.075	13.612	0.409	0.974	0.291	20.234	30.352	0.630
Cd	Langmuir	0.929	0.533	19.610	29.415	0.452	0.995	0.022	3.750	5.625	0.130
	Freundlich	0.902	0.425	14.633	21.950	0.533	0.967	0.255	17.069	25.603	0.322
	Redlich–P.	0.968	0.768	17.688	35.376	0.351	0.995	0.020	3.166	6.332	0.149
	Temkin	0.843	0.650	34.657	51.985	0.672	0.982	0.072	10.730	16.095	0.238
Pb	Langmuir	0.985	3.454	23.968	35.952	0.541	0.995	3.695	17.752	26.628	0.260
	Freundlich	0.983	0.582	17.816	26.724	0.770	0.991	0.524	15.537	23.305	0.340
	Redlich–P.	0.985	5.204	18.873	37.747	0.385	0.995	3.913	17.616	35.231	0.298
	Temkin	0.715	1.864	62.184	93.277	1.547	0.745	2.279	69.045	103.568	1.802
Zn	Langmuir	0.997	0.024	3.449	5.174	0.108	0.923	2.992	15.569	23.354	0.528
	Freundlich	0.957	0.280	14.257	21.386	0.382	0.982	0.059	4.510	6.764	0.257
	Redlich–P.	0.999	0.002	0.890	1.780	0.061	0.982	0.058	4.216	8.432	0.292
	Temkin	0.999	0.004	1.080	1.621	0.066	0.953	0.153	9.107	13.661	0.414

Table 11. Values of competitive affinity (k_{Li}) in the multimetal system.

pH	Composite	$k_{L,As}$	$k_{L,Pb}$	$k_{L,Cd}$	$k_{L,Zn}$
4.5	NR/HMB-HA	0.6163	22.0647	0.9253	1.4653
	NR/HUT-HA	0.7190	5.2763	0.0057	2.4004
5.5	NR/HMB-HA	1.4884	14.6263	0.2958	5.1925
	NR/HUT-HA	0.0020	3.4668	2.2786	2.2984

3.6. Adsorption After Regeneration Cycles

Following chemical regeneration, a progressive decrease is observed, which is characteristic of hybrid adsorbents subjected to repeated adsorption processes. During the first two cycles, the adsorption capacity for both adsorbents is similar (p-value < 0.05) (Figure 6), indicating that treatment with HCl facilitates the release of cations bound to the active sites by strong chemical bonds. Subsequently, a significant decrease is observed, both in percentage and in adsorption capacity (q_e). This can be attributed to the denaturation of the compound functional groups, which bind strongly to intraporous metal ions, leading to the irreversible occupation of active sites, especially those associated with higher energy complexes.

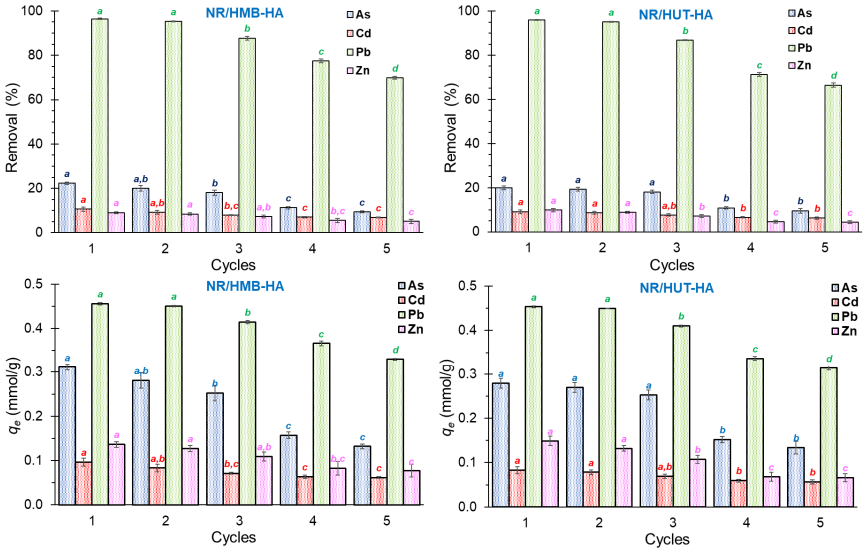


Figure 6. Composite regeneration cycles. Different letters indicate a significant difference at the 5% significance level, assessed using Tukey's test at a significance level of 0.05.

It was also observed that, from the third cycle onwards, the adsorption efficiency of Pb and As decreases considerably, while it is higher for Cd and Zn. For the fifth cycle, Pb removal was reported to be around 0.33 mmol/g (equivalent to between 65 and 70%), while that of As reached around 0.13 mmol/g (approximately 10%), and for Cd and Zn, removal was around 0.06 mmol/g (between 4.4 and 6.8%). Furthermore, NR/HMB-HA shows slightly higher removal in all cycles compared to NR/HUT-HA, indicating greater structural and chemical stability, primarily due to the crystallinity of the activated clay, which would allow for better protection of its chelating functional groups against acid attack. The rapid decrease in adsorption capacity from the third cycle onward confirms that composites exhibit a preference for chemisorption. This behavior is undesirable in many cases because it implies costs associated with replacing the absorbent; and for the present study, it is a challenge to overcome, which allows for further research by adding other synergistic adsorbents to the clay–hydrocolloid mixture [13,120]. This suggests that the application of the studied composites could be aimed at the removal of heavy metals

from drinking water; although in many cases, they are found above permissible limits and are present in low concentrations compared to industrial wastewater.

In general, the characteristics of composites condition adsorption. This is evident because at pH 5.5, which is above pH_{ZCP}, better adsorption yields are reported for the multimetal system, due to the greater affinity for deprotonated sites. In addition, the cation exchange offered by the activated clay and the stability of the adsorbent particles measured by ζ, the degree of crystallization, and the particle size (≈420 nm) allow the formation of the metal–composite complex governed mainly by chemisorption. This behavior is desirable in nanometric adsorbent materials, as it would allow for several regeneration cycles. [22,28,59].

4. Conclusions

Activated HUT and HMB clays showed substantial improvements in their physicochemical properties, reflected in an increase in cation exchange capacity between 300 and 800%, associated with the activation of surface sites and ion exchange with Na^+. These modifications led to ζ values characteristic of high colloidal stability, a greater fraction of nanoscale particles, and a pH at the zero charge point close to 5.1, conditions favorable for the adsorption of metal cations. Atomized nostoc (HA) exhibited a high density of organic functional groups (–OH, –NH, –CO, and –CN), a moderately negative ζ, and a pH_{ZCP} close to 9.0, providing complementary active sites for adsorption. The combination of nostoc and activated clays in composites (20:80, w/w) resulted in materials with a $pH_{ZCP} \approx 5.1$, high colloidal stability, and a highly reactive biological–inorganic hybrid surface. In multimetal systems, the NR/HMB-HA and NR/HUT-HA composites exhibited high adsorption efficiency, especially at pH 5.5, achieving removals greater than 99.6% for Pb^{2+} and significant adsorptions of As^{3+}, Cd^{2+}, and Zn^{2+}. The kinetics revealed a rapid initial stage dominated by chemisorption, followed by a phase controlled by intraporous diffusion, reaching equilibrium in approximately 90 min. The data were mainly fitted to pseudo-second-order and Elovich models, confirming the chemical nature of the process. The equilibrium behavior was adequately described by the Langmuir, Freundlich, Redlich–Peterson, and Temkin models, with high R^2 values and low statistical errors. Isothermal parameters showed favorable adsorption, heterogeneous surfaces, and marked selectivity for Pb^{2+} in both unimetal and multimetal batch systems, confirming that the synergy between the activated clay and the hydrocolloid enhances adsorption efficiency. These results position the developed composites as highly promising materials for the remediation of water contaminated with heavy metals in complex multimetal systems.

Author Contributions: Conceptualization, D.C.-Q., J.W.E.-S., Y.F.C.-M., C.R.C.R. and E.A.L.; methodology, D.C.-Q., Y.G.P.-M. and Y.F.C.-M.; software, W.M.D.B.; validation, J.W.E.-S. and Y.G.P.-M.; formal analysis, D.C.-Q., J.W.E.-S., W.M.D.B. and A.R.B.; investigation, J.W.E.-S., Y.G.P.-M., Y.F.C.-M., B.J.A.A. and E.A.L.; data curation, D.C.-Q.; writing—original draft preparation, D.C.-Q., Y.F.C.-M., A.R.B. and C.E.D.V.; writing—review and editing, D.C.-Q., A.R.B. and C.R.C.R.; visualization, A.R.B., C.R.C.R. and E.A.L.; supervision, E.A.L.; project administration, D.C.-Q. and B.J.A.A. All authors have read and agreed to the published version of the manuscript.

Funding: This research received no external funding. The APC was funded by the authors.

Data Availability Statement: The data presented in this study are available in this article or can be requested from the corresponding author.

Acknowledgments: The authors would like to acknowledge the Laboratory of Research in Materials for Water and Food Treatment (LIMTA), and the Research Vice-Rectorate of the José María Arguedas National University. Laboratory of the Experimental Center for Ceramics at the National University of San Cristóbal de Huamanga, Ayacucho, Peru.

Conflicts of Interest: The authors declare no conflicts of interest.

References

1. Kumar, P.S.; Ramalingam, S.; Sathyaselvabala, V.; Kirupha, S.D.; Murugesan, A.; Sivanesan, S. Removal of cadmium (II) from aqueous solution by agricultural waste cashew nut shell. *Korean J. Chem. Eng.* **2012**, *29*, 756–768. [CrossRef]
2. Rubio, D.I.C.; Calderón, R.A.M.; Gualtero, A.P.; Acosta, D.R.; Sandoval, J. Treatments for Removal of Heavy Metals Commonly Found in Industrial Wastewater. A Review. Una revisión. *Ing. Región* **2015**, *13*, 73–90.
3. Tejada-Tovar, C.; Villabona-Ortiz, Á.; Garcés-Jaraba, L. Adsorption of heavy metals in waste water using biological materials. *TecnoLógicas* **2015**, *18*, 109–123. [CrossRef]
4. Esmaeili, A.; Khoshnevisan, N. Optimization of process parameters for removal of heavy metals by biomass of Cu and Co-doped alginate-coated chitosan nanoparticles. *Bioresour. Technol.* **2016**, *218*, 650–658. [CrossRef] [PubMed]
5. Malayoglu, U. Removal of heavy metals by biopolymer (chitosan)/nanoclay composites. *Sep. Sci. Technol.* **2018**, *53*, 2741–2749. [CrossRef]
6. Rentería-Villalobos, M.; Marfil, L.R.; Palma, N.A.; Arias, H.R.; Álvarez, C.P.; Verín, C.V.S. Lead removal in aqueous solution using orange peel (*Citrus sinensis*). *Investig. Y Cienc. Univ. Autónoma Aguascalientes* **2014**, *62*, 5–10.
7. Borja, N.; García Villegas, V.; Yipmantin-Ojeda, A.; Guzmán Lezama, E.; Maldonado García, H. Kinetic study of lead (II) biosorption on Ascophyllum nodosum seaweed. *Rev. Soc. Química Perú* **2015**, *81*, 212–223.
8. Efimova, N.V.; Krasnopyorova, A.P.; Yuhno, G.D.; Scheglovskaya, A.A. Sorption of heavy metals by natural biopolymers. *Adsorpt. Sci. Technol.* **2017**, *35*, 595–601. [CrossRef]
9. Rani, K.; Gomathi, T.; Vijayalakshmi, K.; Saranya, M.; Sudha, P.N. Banana fiber Cellulose Nano Crystals grafted with butyl acrylate for heavy metal lead (II) removal. *Int. J. Biol. Macromol.* **2019**, *131*, 461–472. [CrossRef]
10. Saravanan, D.; Sudha, P.N. Batch adsorption studies for the removal of copper from wastewater using natural biopolymer. *Int. J. ChemTech Res.* **2014**, *6*, 3496–3508.
11. Atoku, D.I.; Ojekunle, O.Z.; Taiwo, A.M.; Shittu, O.B. Evaluating the efficiency of Nostoc commune, Oscillatoria limosa and Chlorella vulgaris in a phycoremediation of heavy metals contaminated industrial wastewater. *Sci. Afr.* **2021**, *12*, e00817. [CrossRef]
12. Mahlangu, D.; Mphahlele, K.; De Paola, F.; Mthombeni, N.H. Microalgae-mediated biosorption for effective heavy metals removal from wastewater: A review. *Water* **2024**, *16*, 718. [CrossRef]
13. Kinoti, I.K.; Karanja, E.M.; Nthiga, E.W.; M'thiruaine, C.M.; Marangu, J.M. Review of clay-based nanocomposites as adsorbents for the removal of heavy metals. *J. Chem.* **2022**, *2022*, 7504626. [CrossRef]
14. Ponce, E. Nostoc: Un alimento diferente y su presencia en la precordillera de Arica. *Idesia* **2014**, *32*, 119–121. [CrossRef]
15. Dinh, L.X.; Van Tung, N.; Lien, N.T.; Minh, P.T.; Le, T.-H. The adsorption kinetic and isotherm studies of metal ions (Co^{2+}, Sr^{2+}, Cs^{+}) on Fe_3O_4 nanoparticle of radioactive importance. *Results Chem.* **2023**, *6*, 101095.
16. Wang, J.; Guo, X. Adsorption kinetics and isotherm models of heavy metals by various adsorbents: An overview. *Crit. Rev. Environ. Sci. Technol.* **2023**, *53*, 1837–1865. [CrossRef]
17. Choque-Quispe, D.; Ligarda-Samanez, C.A.; Choque-Quispe, Y.; Solano-Reynoso, A.M.; Ramos-Pacheco, B.S.; Zamalloa-Puma, M.M.; Álvarez-López, G.J.; Zamalloa-Puma, A.; Choque-Quispe, K.; Alzamora-Flores, H. Multimetal removal in aqueous medium using a potato starch/nopal mucilage copolymer: A study of adsorption kinetics and isotherms. *Results Eng.* **2023**, *18*, 101164. [CrossRef]
18. Abbas, A.; Siddique, A.B.; Batool, R.; Sher, M.; Irfan, M.I.; Abbas, M.A. Isothermal and kinetic modeling for uptake of heavy metal ion from aqueous solution using succinylated polysaccharide. *Starch-Stärke* **2023**, *75*, 2200191. [CrossRef]
19. Kosmulski, M. *Surface Charging and Points of Zero Charge*; CRC Press: Boca Raton, FL, USA, 2009.
20. Choi, H.-J.; Yu, S.-W.; Kim, K.H. Efficient use of Mg-modified zeolite in the treatment of aqueous solution contaminated with heavy metal toxic ions. *J. Taiwan Inst. Chem. Eng.* **2016**, *63*, 482–489. [CrossRef]
21. Al Mahrouqi, D.; Vinogradov, J.; Jackson, M.D. Zeta potential of artificial and natural calcite in aqueous solution. *Adv. Colloid Interface Sci.* **2017**, *240*, 60–76. [CrossRef]
22. Yang, Y.; Liu, M.; Tang, S.; You, X.; Li, Y.; Mei, Y.; Chen, Y. Investigation of the key mechanisms and optimum conditions of high-effective phosphate removal by bimetallic La-Fe-CNT film. *Sep. Purif. Technol.* **2024**, *341*, 126938. [CrossRef]
23. Choque-Quispe, D.; Mojo-Quisani, A.; Ligarda-Samanez, C.A.; Calla-Florez, M.; Ramos-Pacheco, B.S.; Zamalloa-Puma, L.M.; Peralta-Guevara, D.E.; Solano-Reynoso, A.M.; Choque-Quispe, Y.; Zamalloa-Puma, A. Preliminary characterization of a spray-dried hydrocolloid from a high Andean algae (*Nostoc sphaericum*). *Foods* **2022**, *11*, 1640. [CrossRef] [PubMed]
24. Jaremko, D.; Kalembasa, D. A comparison of methods for the determination of cation exchange capacity of soils/Porównanie metod oznaczania pojemności wymiany kationów i sumy kationów wymiennych w glebach. *Ecol. Chem. Eng. S* **2014**, *21*, 487–498. [CrossRef]

25. Fonseca, A.F.d.; Alleoni, L.R.F.; Melfi, A.J.; Montes, C.R. Cation exchange capacity of an Oxisol amended with an effluent from domestic sewage treatment. *Sci. Agric.* **2005**, *62*, 552–558. [CrossRef]
26. Ligarda-Samanez, C.A.; Choque-Quispe, D.; Palomino-Rincón, H.; Ramos-Pacheco, B.S.; Moscoso-Moscoso, E.; Huamán-Carrión, M.L.; Peralta-Guevara, D.E.; Obregón-Yupanqui, M.E.; Aroni-Huamán, J.; Bravo-Franco, E.Y.; et al. Modified Polymeric Biosorbents from Rumex acetosella for the Removal of Heavy Metals in Wastewater. *Polymers* **2022**, *14*, 2191. [CrossRef] [PubMed]
27. Dome, K.; Podgorbunskikh, E.; Bychkov, A.; Lomovsky, O. Changes in the crystallinity degree of starch having different types of crystal structure after mechanical pretreatment. *Polymers* **2020**, *12*, 641. [CrossRef]
28. Monshi, A.; Foroughi, M.R.; Monshi, M.R. Modified Scherrer equation to estimate more accurately nano-crystallite size using XRD. *World J. Nano Sci. Eng.* **2012**, *2*, 154–160. [CrossRef]
29. Singha, A.S.; Guleria, A. Chemical modification of cellulosic biopolymer and its use in removal of heavy metal ions from wastewater. *Int. J. Biol. Macromol.* **2014**, *67*, 409–417. [CrossRef]
30. Tseng, R.-L.; Wu, F.-C.; Juang, R.-S. Characteristics and applications of the Lagergren's first-order equation for adsorption kinetics. *J. Taiwan Inst. Chem. Eng.* **2010**, *41*, 661–669. [CrossRef]
31. Ho, Y.S.; McKay, G. A comparison of chemisorption kinetic models applied to pollutant removal on various sorbents. *Process Saf. Environ. Prot.* **1998**, *76*, 332–340. [CrossRef]
32. Ho, Y.-S.; McKay, G. Pseudo-second order model for sorption processes. *Process Biochem.* **1999**, *34*, 451–465. [CrossRef]
33. Blanchard, G.; Maunaye, M.; Martin, G. Removal of heavy metals from waters by means of natural zeolites. *Water Res.* **1984**, *18*, 1501–1507. [CrossRef]
34. Cheung, C.W.; Porter, J.F.; McKay, G. Sorption kinetic analysis for the removal of cadmium ions from effluents using bone char. *Water Res.* **2001**, *35*, 605–612. [CrossRef] [PubMed]
35. Plazinski, W.; Dziuba, J.; Rudzinski, W. Modeling of sorption kinetics: The pseudo-second order equation and the sorbate intraparticle diffusivity. *Adsorption* **2013**, *19*, 1055–1064. [CrossRef]
36. Wang, J.; Guo, X. Rethinking of the intraparticle diffusion adsorption kinetics model: Interpretation, solving methods and applications. *Chemosphere* **2022**, *309*, 136732. [CrossRef]
37. Oyelude, E.O.; Awudza, J.A.M.; Twumasi, S.K. Removal of malachite green from aqueous solution using pulverized teak leaf litter: Equilibrium, kinetic and thermodynamic studies. *Chem. Cent. J.* **2018**, *12*, 81. [CrossRef]
38. Largitte, L.; Pasquier, R. A review of the kinetics adsorption models and their application to the adsorption of lead by an activated carbon. *Chem. Eng. Res. Des.* **2016**, *109*, 495–504. [CrossRef]
39. Crank, J. *The Mathematics of Diffusion*; Oxford University Press: Oxford, UK, 1979.
40. Ho, Y.-S.; McKay, G. Sorption of dye from aqueous solution by peat. *Chem. Eng. J.* **1998**, *70*, 115–124. [CrossRef]
41. Igwe, J.C. A review of potentially low cost sorbents for heavy metal removal and recovery. *Terr. Aquat. Environ. Toxicol.* **2007**, *1*, 60–69.
42. Ramachandran, P.; Vairamuthu, R.; Ponnusamy, S. Adsorption isotherms, kinetics, thermodynamics and desorption studies of reactive Orange 16 on activated carbon derived from *Ananas comosus* (L.) carbon. *J. Eng. Appl. Sci.* **2011**, *6*, 15–26.
43. Seliem, M.K.; Komarneni, S.; Byrne, T.; Cannon, F.S.; Shahien, M.G.; Khalil, A.A.; Abd El-Gaid, I.M. Removal of nitrate by synthetic organosilicas and organoclay: Kinetic and isotherm studies. *Sep. Purif. Technol.* **2013**, *110*, 181–187. [CrossRef]
44. Redlich, O.; Peterson, D.L. A useful adsorption isotherm. *J. Phys. Chem.* **1959**, *63*, 1024. [CrossRef]
45. Vadi, M.; Salmanpour, M.; Bolqar, S. Investigation of Langmuir, Freundlich and Temkin isotherms of Letrozole by single-wall carbon nanotube and multi-wall carbon nanotube. *Res. J. Pharm. Biol. Chem. Sci.* **2014**, *5*, 52–56.
46. Shikuku, V.O.; Mishra, T. Adsorption isotherm modeling for methylene blue removal onto magnetic kaolinite clay: A comparison of two-parameter isotherms. *Appl. Water Sci.* **2021**, *11*, 103. [CrossRef]
47. Abbou, B.; Lebkiri, I.; Ouaddari, H.; Kadiri, L.; Ouass, A.; Habsaoui, A.; Lebkiri, A.; Rifi, E.H. Removal of Cd(II), Cu(II), and Pb(II) by adsorption onto natural clay: A kinetic and thermodynamic study. *Turk. J. Chem.* **2021**, *45*, 362–376. [CrossRef]
48. Auta, M.; Hameed, B.H. Chitosan–clay composite as highly effective and low-cost adsorbent for batch and fixed-bed adsorption of methylene blue. *Chem. Eng. J.* **2014**, *237*, 352–361. [CrossRef]
49. Carhuarupay-Molleda, Y.F.; Ccasa Barboza, N.M.; Pastor-Mina, S.; Dueñas Valcarcel, C.E.; Palomino-Malpartida, Y.G.; Licapa Redolfo, R.; Mojo-Quisani, A.; Calla-Florez, M.; Aguilar-Salazar, R.F.; Flores-Ccorisapra, Y. A Study of Methylene Blue Adsorption by a Synergistic Adsorbent Algae (Nostoc sphaericum)/Activated Clay. *Polymers* **2025**, *17*, 2134. [CrossRef]
50. Emiola, I.; Adem, R. Comparison of Minimization Methods for Rosenbrock Functions. In Proceedings of the 2021 29th Mediterranean Conference on Control and Automation (MED), Virtually, 22–25 June 2021; pp. 837–842.
51. Zhang, F.; Tang, X.; Huang, Y.; Keller, A.A.; Lan, J. Competitive removal of Pb^{2+} and malachite green from water by magnetic phosphate nanocomposites. *Water Res.* **2019**, *150*, 442–451. [CrossRef]
52. Moroi, G.-N.; Avram, E.; Bulgariu, L. Adsorption of Heavy Metal Ions onto Surface-Functionalised Polymer Beads. I. Modelling of Equilibrium Isotherms by Using Non-Linear and Linear Regression Analysis. *Water Air Soil Pollut.* **2016**, *227*, 260. [CrossRef]

53. Popoola, L.T.; Yusuff, A.S.; Adesina, O.A.; Lala, M.A. Brilliant green dye sorption onto snail shell-rice husk: Statistical and error function models as parametric isotherm predictors. *J. Environ. Sci. Technol.* **2019**, *12*, 65–80. [CrossRef]
54. Zgorelec, Z.; Grahovac, B.; Percin, A.; Jurkovic, V.; Gandjaeva, L.; Maurovic, N. Comparison of two different CEC determination methods regarding the soil properties. *Agric. Conspec. Sci.* **2019**, *84*, 151–158.
55. Aran, D.; Maul, A.; Masfaraud, J.-F. A spectrophotometric measurement of soil cation exchange capacity based on cobaltihexamine chloride absorbance. *Comptes Rendus Geosci.* **2008**, *340*, 865–871. [CrossRef]
56. Do Rosário, J.A.; Miguel, R.F.; Do Rosário, D.A.; Kuhnen, N.C.; Riella, H.G. Factorial design applied to sodium activation of a Brazilian bentonite. *Cerâmica* **2019**, *65*, 185–189. [CrossRef]
57. Fyodorov, M.V.; Seredin, V.V.; Lunegov, I.V. *Change in the Adhesion Force of Clay Soils Modified by Hydrochloric Acid and Pressure*; Springer International Publishing: Cham, Switzerland, 2022; pp. 236–244.
58. Khalifa, A.Z.; Cizer, Ö.; Pontikes, Y.; Heath, A.; Patureau, P.; Bernal, S.A.; Marsh, A.T.M. Advances in alkali-activation of clay minerals. *Cem. Concr. Res.* **2020**, *132*, 106050. [CrossRef]
59. Makhoukhi, B.; Didi, M.A.; Villemin, D.; Azzouz, A. Acid activation of Bentonite for use as a vegetable oil bleaching agent. *Grasas Y Aceites* **2009**, *60*, 343–349. [CrossRef]
60. Zhang, Y.; Jiang, T.; Chen, L.; Li, G. Study on sodium modification of inferior Ca-Based bentonite by suspension method. *Int. Sch. Res. Not.* **2011**, *2011*, 953132. [CrossRef]
61. Djebbar, M.; Djafri, F.; Bouchekara, M.; Djafri, A. Adsorption of phenol on natural clay. *Appl. Water Sci.* **2012**, *2*, 77–86. [CrossRef]
62. Kaya, A.; Yukselen, Y. Zeta potential of clay minerals and quartz contaminated by heavy metals. *Can. Geotech. J.* **2005**, *42*, 1280–1289. [CrossRef]
63. Yukselen, Y.; Kaya, A. Zeta potential of kaolinite in the presence of alkali, alkaline earth and hydrolyzable metal ions. *Water Air Soil Pollut.* **2003**, *145*, 155–168. [CrossRef]
64. Fijałkowska, G.; Wiśniewska, M.; Szewczuk-Karpisz, K.; Jędruchniewicz, K.; Oleszczuk, P. Comparison of lead (II) ions accumulation and bioavailability on the montmorillonite and kaolinite surfaces in the presence of polyacrylamide soil flocculant. *Chemosphere* **2021**, *276*, 130088. [CrossRef]
65. Agnihotri, S.; Mukherji, S.; Mukherji, S. Size-controlled silver nanoparticles synthesized over the range 5–100 nm using the same protocol and their antibacterial efficacy. *RSC Adv.* **2014**, *4*, 3974–3983. [CrossRef]
66. Souza, T.G.F.; Ciminelli, V.S.T.; Mohallem, N.D.S. *A Comparison of TEM and DLS Methods to Characterize Size Distribution of Ceramic Nanoparticles*; IOP Publishing: Bristol, UK, 2016; p. 012039.
67. Singh, S.; Bothara, S.B. Physico-chemical and structural characterization of mucilage isolated from seeds of Diospyros melonoxylon Roxb. *Braz. J. Pharm. Sci.* **2014**, *50*, 713–725. [CrossRef]
68. Lin, J.; Cai, X.; Tang, M.; Wang, S. Preparation and evaluation of the chelating nanocomposite fabricated with marine algae *Schizochytrium* sp. protein hydrolysate and calcium. *J. Agric. Food Chem.* **2015**, *63*, 9704–9714. [CrossRef]
69. Tuesta, E.G.; Vivas, M.; Sun, R.; Gutarra, A. Modificación química de arcillas y su aplicación en la retención de colorantes. *Rev. Soc. Química Peru* **2005**, *71*, 26–36.
70. Novikova, L.; Ayrault, P.; Fontaine, C.; Chatel, G.; Jérôme, F.; Belchinskaya, L. Effect of low frequency ultrasound on the surface properties of natural aluminosilicates. *Ultrason. Sonochemistry* **2016**, *31*, 598–609. [CrossRef]
71. Putro, J.N.; Lunardi, V.B.; Soetaredjo, F.E.; Yuliana, M.; Santoso, S.P.; Wenten, I.G.; Ismadji, S. A review of gum hydrocolloid polyelectrolyte complexes (Pec) for biomedical applications: Their properties and drug delivery studies. *Processes* **2021**, *9*, 1796. [CrossRef]
72. Es-Sahbany, H.; Hsissou, R.; El Hachimi, M.L.; Allaoui, M.; Nkhili, S.; Elyoubi, M.S. Investigation of the adsorption of heavy metals (Cu, Co, Ni and Pb) in treatment synthetic wastewater using natural clay as a potential adsorbent (Sale-Morocco). *Mater. Today Proc.* **2021**, *45*, 7290–7298. [CrossRef]
73. Bedelean, H.; Măicăneanu, A.; Burcă, S.; Stanca, M. Removal of heavy metal ions from wastewaters using natural clays. *Clay Miner.* **2009**, *44*, 487–495. [CrossRef]
74. Macías-Quiroga, I.F.; Giraldo-Gómez, G.I.; Sanabria-González, N.R. Characterization of Colombian clay and its potential use as adsorbent. *Sci. World J.* **2018**, *2018*, 5969178. [CrossRef] [PubMed]
75. Pawar, R.R.; Lalhmunsiama; Bajaj, H.C.; Lee, S.-M. Activated bentonite as a low-cost adsorbent for the removal of Cu(II) and Pb(II) from aqueous solutions: Batch and column studies. *J. Ind. Eng. Chem.* **2016**, *34*, 213–223. [CrossRef]
76. Barquilha, C.E.R.; Cossich, E.S.; Tavares, C.R.G.; Silva, E.A. Biosorption of nickel (II) and copper (II) ions by *Sargassum* sp. in nature and alginate extraction products. *Bioresour. Technol. Rep.* **2019**, *5*, 43–50. [CrossRef]
77. Liu, X.; Chen, Z.-Q.; Han, B.; Su, C.-L.; Han, Q.; Chen, W.-Z. Biosorption of copper ions from aqueous solution using rape straw powders: Optimization, equilibrium and kinetic studies. *Ecotoxicol. Environ. Saf.* **2018**, *150*, 251–259. [CrossRef]
78. Kokate, S.; Parasuraman, K.; Prakash, H. Adsorptive removal of lead ion from water using banana stem scutcher generated in fiber extraction process. *Results Eng.* **2022**, *14*, 100439. [CrossRef]

79. Kollannur Nikhil, J.; Arnepalli Dali, N. Methodology for Determining Point of Zero Salt Effect of Clays in Terms of Surface Charge Properties. *J. Mater. Civ. Eng.* **2019**, *31*, 04019286. [CrossRef]
80. Drweesh, S.A.; Fathy, N.A.; Wahba, M.A.; Hanna, A.A.; Akarish, A.I.M.; Elzahany, E.A.M.; El-Sherif, I.Y.; Abou-El-Sherbini, K.S. Equilibrium, kinetic and thermodynamic studies of Pb(II) adsorption from aqueous solutions on HCl-treated Egyptian kaolin. *J. Environ. Chem. Eng.* **2016**, *4*, 1674–1684. [CrossRef]
81. Zhou, D.; Zhang, L.; Zhou, J.; Guo, S. Cellulose/chitin beads for adsorption of heavy metals in aqueous solution. *Water Res.* **2004**, *38*, 2643–2650. [CrossRef] [PubMed]
82. Kuo, C.-Y.; Wu, C.-H.; Chen, M.-J. Adsorption of lead ions from aqueous solutions by citric acid-modified celluloses. *Desalination Water Treat.* **2015**, *55*, 1264–1270. [CrossRef]
83. Abou-Zeid, R.E.; Dacrory, S.; Ali, K.A.; Kamel, S. Novel method of preparation of tricarboxylic cellulose nanofiber for efficient removal of heavy metal ions from aqueous solution. *Int. J. Biol. Macromol.* **2018**, *119*, 207–214. [CrossRef] [PubMed]
84. Liu, G.; Liao, L.; Dai, Z.; Qi, Q.; Wu, J.; Ma, L.Q.; Tang, C.; Xu, J. Organic adsorbents modified with citric acid and Fe_3O_4 enhance the removal of Cd and Pb in contaminated solutions. *Chem. Eng. J.* **2020**, *395*, 125108. [CrossRef]
85. Bui, T.H.; Pham, V.S.; Thanh-Nho, N.; Trieu, Q.A. Removal of arsenic from water using a composite of iron–manganese oxide incorporated active rice husk silica. *CLEAN–Soil Air Water* **2021**, *49*, 2000233. [CrossRef]
86. Mangood, A.H.; El-Saied, F.A.; El-shinawy, F.H.; Abo-Elenan, S.A. Metals Removal from Contaminated Aqueous Medium by Using Modified Cellulose-N (4)-Antipyrinyl Thiosemicarbazide. *Polycycl. Aromat. Compd.* **2023**, *44*, 1760–1780. [CrossRef]
87. Ismael, I.S.; Melegy, A.; Kratochvíl, T. Lead removal from aqueous solution by natural and pretreated zeolites. *Geotech. Geol. Eng.* **2012**, *30*, 253–262. [CrossRef]
88. Pawar, R.R.; Kim, M.; Kim, J.-G.; Hong, S.-M.; Sawant, S.Y.; Lee, S.M. Efficient removal of hazardous lead, cadmium, and arsenic from aqueous environment by iron oxide modified clay-activated carbon composite beads. *Appl. Clay Sci.* **2018**, *162*, 339–350. [CrossRef]
89. Okpara, O.G.; Ogbeide, O.M.; Nworu, J.N.; Chukwuekeh, J.I.; Igoche, S.A.; Alichi, F.S.; Orinya, O.E. Enhanced Removal of Pb (II), Cd (II), and Zn (II) Ions from Aqueous Solutions Using EDTA-Synthesized Activated Carbon Derived from Sawdust. *Open Access Libr. J.* **2023**, *10*, 1–15. [CrossRef]
90. Alkherraz, A.M.; Ali, A.K.; Elsherif, K.M. Removal of Pb (II), Zn (II), Cu (II) and Cd (II) from aqueous solutions by adsorption onto olive branches activated carbon: Equilibrium and thermodynamic studies. *Chem. Int.* **2020**, *6*, 11–20.
91. Zendelska, A.; Golomeova, M. Effect of competing cations (Cu, Zn, Mn, Pb) adsorbed by natural zeolite. *Int. J. Sci. Eng. Technol.* **2014**, *2*, 483–492.
92. Šuránek, M.; Melichová, Z.; Kureková, V.; Kljajević, L.; Nenadović, S. Removal of Nickel from Aqueous Solutions by Natural Bentonites from Slovakia. *Materials* **2021**, *14*, 282. [CrossRef]
93. Alexander, J.A.; Zaini, M.A.A.; Abdulsalam, S.; Aliyu El-Nafaty, U.; Aroke, U.O. Isotherm studies of lead (II), manganese (II), and cadmium (II) adsorption by Nigerian bentonite clay in single and multimetal solutions. *Part. Sci. Technol.* **2019**, *37*, 403–413. [CrossRef]
94. Mohamed Ziyath, A.; Mahbub, P.; Goonetilleke, A.; Adebajo, M.; Kokot, S.; Oloyede, A. Influence of physical and chemical parameters on the treatment of heavy metals in polluted stormwater using zeolite-a review. *J. Water Resour. Prot.* **2011**, *3*, 758–767. [CrossRef]
95. Ramos, D.C. Cadmium, Copper and Lead Adsorption on Natural and Modified Bentonite, Kaolin and Zeolite: A Review of Process Parameters, Isotherms and Kinetics. *Rev. Ing.* **2018**, *23*, 252–273.
96. Alandis, N.M.; Aldayel, O.A.; Mekhemer, W.K.; Hefne, J.A.; Jokhab, H.A. Thermodynamic and kinetic studies for the adsorption of Fe (III) and Ni (II) ions from aqueous solution using natural bentonite. *J. Dispers. Sci. Technol.* **2010**, *31*, 1526–1534. [CrossRef]
97. Al Juhaiman, L.A.; Al-Enezi, D.A.; Mekhamer, W.K. Preparation and characterization of polystyrene/organoclay nanocomposites from raw clay. *Dig. J. Nanomater. Biostruct* **2016**, *11*, 105–114.
98. Śliwińska, A.; Smolinski, A.; Kucharski, P. Simultaneous analysis of heavy metal concentration in soil samples. *Appl. Sci.* **2019**, *9*, 4705. [CrossRef]
99. Mamera, M.; van Tol, J.J.; Aghoghovwia, M.P.; Kotze, E. Sensitivity and calibration of the FT-IR spectroscopy on concentration of heavy metal ions in river and borehole water sources. *Appl. Sci.* **2020**, *10*, 7785. [CrossRef]
100. Gupta, S.S.; Bhattacharyya, K.G. Immobilization of Pb (II), Cd (II) and Ni (II) ions on kaolinite and montmorillonite surfaces from aqueous medium. *J. Environ. Manag.* **2008**, *87*, 46–58. [CrossRef] [PubMed]
101. Matouq, M.; Jildeh, N.; Qtaishat, M.; Hindiyeh, M.; Al Syouf, M.Q. The adsorption kinetics and modeling for heavy metals removal from wastewater by Moringa pods. *J. Environ. Chem. Eng.* **2015**, *3*, 775–784. [CrossRef]
102. Yang, J.; Hou, B.; Wang, J.; Tian, B.; Bi, J.; Wang, N.; Li, X.; Huang, X. Nanomaterials for the removal of heavy metals from wastewater. *Nanomaterials* **2019**, *9*, 424. [CrossRef] [PubMed]
103. Wang, J.; Zhang, W. Evaluating the adsorption of Shanghai silty clay to Cd(II), Pb(II), As(V), and Cr(VI): Kinetic, equilibrium, and thermodynamic studies. *Environ. Monit. Assess.* **2021**, *193*, 131. [CrossRef]

104. Kocaoba, S.; Arısoy, M. Biosorption of cadmium (II) and lead (II) from aqueous solutions using Pleurotus ostreatus immobilized on bentonite. *Sep. Sci. Technol.* **2018**, *53*, 1703–1710. [CrossRef]
105. Diniz, V.; Volesky, B. Effect of counterions on lanthanum biosorption by *Sargassum polycystum*. *Water Res.* **2005**, *39*, 2229–2236. [CrossRef]
106. Alexander, J.A.; Surajudeen, A.; Aliyu, E.-N.U.; Omeiza, A.U.; Zaini, M.A.A. Multi-metals column adsorption of lead (II), cadmium (II) and manganese (II) onto natural bentonite clay. *Water Sci. Technol.* **2017**, *76*, 2232–2241. [CrossRef]
107. Kozera-Sucharda, B.; Gworek, B.; Kondzielski, I. The Simultaneous Removal of Zinc and Cadmium from Multicomponent Aqueous Solutions by Their Sorption onto Selected Natural and Synthetic Zeolites. *Minerals* **2020**, *10*, 343. [CrossRef]
108. Barquilha, C.E.R.; Cossich, E.S.; Tavares, C.R.G.; Silva, E.A. Biosorption of nickel (II) and copper (II) ions in batch and fixed-bed columns by free and immobilized marine algae Sargassum sp. *J. Clean. Prod.* **2017**, *150*, 58–64. [CrossRef]
109. Kozera-Sucharda, B.; Gworek, B.; Kondzielski, I.; Chojnicki, J. The Comparison of the Efficacy of Natural and Synthetic Aluminosilicates, Including Zeolites, in Concurrent Elimination of Lead and Copper from Multi-Component Aqueous Solutions. *Processes* **2021**, *9*, 812. [CrossRef]
110. Rajeshwari, K.; Latha, S.; Gomathi, T.; Sangeetha, K.; Sudha, P.N. Adsorption of Heavy Metal Cr (VI) by a Ternary Biopolymer Blend. *Mater. Today Proc.* **2018**, *5*, 14628–14638. [CrossRef]
111. Foo, K.Y.; Hameed, B.H. Insights into the modeling of adsorption isotherm systems. *Chem. Eng. J.* **2010**, *156*, 2–10. [CrossRef]
112. Baláž, P.; Aláčová, A.; Briančin, J. Sensitivity of Freundlich equation constant 1/n for zinc sorption on changes induced in calcite by mechanical activation. *Chem. Eng. J.* **2005**, *114*, 115–121. [CrossRef]
113. Allen, S.J.; McKay, G.; Porter, J.F. Adsorption isotherm models for basic dye adsorption by peat in single and binary component systems. *J. Colloid Interface Sci.* **2004**, *280*, 322–333. [CrossRef]
114. Stepova, K.; Sysa, L.; Konanets, R. Nonlinear Fitting of Iron Sorption on Bentonite to Theoretical Isotherm Models. *Phys. Chem. Solid State* **2022**, *23*, 270–276. [CrossRef]
115. Tran, H.N.; Lima, E.C.; Juang, R.-S.; Bollinger, J.-C.; Chao, H.-P. Thermodynamic parameters of liquid–phase adsorption process calculated from different equilibrium constants related to adsorption isotherms: A comparison study. *J. Environ. Chem. Eng.* **2021**, *9*, 106674. [CrossRef]
116. Chu, K.H. Revisiting the Temkin isotherm: Dimensional inconsistency and approximate forms. *Ind. Eng. Chem. Res.* **2021**, *60*, 13140–13147. [CrossRef]
117. Seyfi, S.; Azadmehr, A.R.; Maghsoudi, A. Comparative and competitive adsorption of Cu (II) and Cd (II) using scoria: Equilibrium, kinetic and thermodynamic studies. *Chem. Res. Chin. Univ.* **2017**, *33*, 471–478. [CrossRef]
118. Shojaeipoor, F.; Elhamifar, D.; Moshkelgosha, R.; Masoumia, B. Removal of Pb (II) and Co (II) ions from aqueous solution and industrial wastewater using ILNO-NH2: Kinetic, isotherm and thermodynamic studies. *J. Taiwan Inst. Chem. Eng.* **2016**, *67*, 166–173. [CrossRef]
119. Vaszilcsin, C.G.; Putz, M.V.; Kellenberger, A.; Dan, M.L. On the evaluation of metal-corrosion inhibitor interactions by adsorption isotherms. *J. Mol. Struct.* **2023**, *1286*, 135643. [CrossRef]
120. Shahadat, M.; Isamil, S. Regeneration performance of clay-based adsorbents for the removal of industrial dyes: A review. *RSC Adv.* **2018**, *8*, 24571–24587. [CrossRef] [PubMed]

Disclaimer/Publisher's Note: The statements, opinions and data contained in all publications are solely those of the individual author(s) and contributor(s) and not of MDPI and/or the editor(s). MDPI and/or the editor(s) disclaim responsibility for any injury to people or property resulting from any ideas, methods, instructions or products referred to in the content.